Molecular Cell

Article

Transcription factors TEAD2 and E2A globally repress acetyl-CoA synthesis to promote tumorigenesis

Graphical abstract

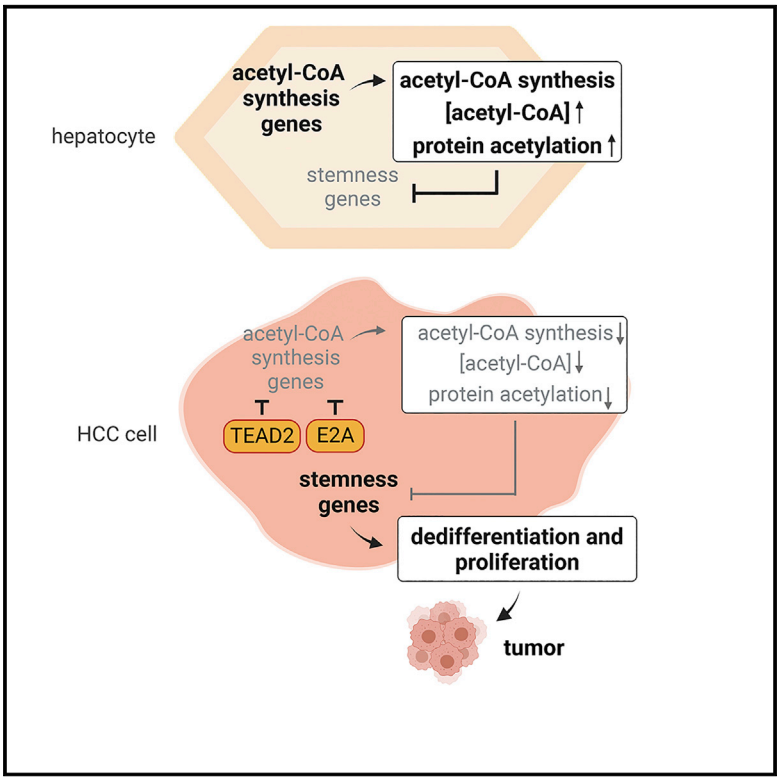

Highlights

- Acetyl-CoA levels and non-histone protein acetylation are decreased in HCC
- All six acetyl-CoA synthesis pathways are transcriptionally downregulated in HCC
- Acetyl-CoA synthesis genes are globally repressed by transcription factors TEAD2 and E2A
- TEAD2 and E2A promote proliferation and dedifferentiation by reducing acetyl-CoA levels

Authors

Sujin Park, Dirk Mossmann, Qian Chen, ..., Luigi M. Terracciano, Markus H. Heim, Michael N. Hall

Correspondence

m.hall@unibas.ch

In brief

Park et al. demonstrate that TEAD2 and E2A transcriptionally repress acetyl-CoA synthesis in HCC, which results in reduced acetylation specifically of non-histone proteins. The authors show that repression of acetyl-CoA synthesis, in turn, promotes oncogenic dedifferentiation and proliferation.

Park et al., 2022, Molecular Cell *82*, 4246–4261
November 17, 2022
https://doi.org/10.1016/j.molcel.2022.10.027

CellPress

CellPress

Molecular Cell

Article

Transcription factors TEAD2 and E2A globally repress acetyl-CoA synthesis to promote tumorigenesis

Sujin Park,[1,7] Dirk Mossmann,[1] Qian Chen,[2,3] Xueya Wang,[2,3] Eva Dazert,[1] Marco Colombi,[1] Alexander Schmidt,[1] Brendan Ryback,[4] Charlotte K.Y. Ng,[5,6] Luigi M. Terracciano,[5,8] Markus H. Heim,[2,3] and Michael N. Hall[1,9,*]

[1]Biozentrum, University of Basel, 4056 Basel, Switzerland
[2]Department of Biomedicine, University of Basel, 4031 Basel, Switzerland
[3]Division of Gastroenterology and Hepatology, Clarunis, University Center for Gastrointestinal and Liver Diseases, 4031 Basel, Switzerland
[4]Institute of Molecular Systems Biology, ETH Zurich, 8093 Zurich, Switzerland
[5]Institute of Pathology, University Hospital Basel, 4031 Basel, Switzerland
[6]Department for BioMedical Research (DBMR), University of Bern, Bern, Switzerland
[7]Present address: Center for Genome Engineering, Institute for Basic Science, 55, Expo-ro, Yuseong-gu, Daejeon 34126, Republic of Korea
[8]Present address: Humanitas University, Department of Biomedical Sciences and Department of Pathology, Humanitas Clinical and Research Center, IRCCS, Milan, Italy
[9]Lead contact
*Correspondence: m.hall@unibas.ch
https://doi.org/10.1016/j.molcel.2022.10.027

SUMMARY

Acetyl-coenzyme A (acetyl-CoA) plays an important role in metabolism, gene expression, signaling, and other cellular processes via transfer of its acetyl group to proteins and metabolites. However, the synthesis and usage of acetyl-CoA in disease states such as cancer are poorly characterized. Here, we investigated global acetyl-CoA synthesis and protein acetylation in a mouse model and patient samples of hepatocellular carcinoma (HCC). Unexpectedly, we found that acetyl-CoA levels are decreased in HCC due to transcriptional downregulation of all six acetyl-CoA biosynthesis pathways. This led to hypo-acetylation specifically of non-histone proteins, including many enzymes in metabolic pathways. Importantly, repression of acetyl-CoA synthesis promoted oncogenic dedifferentiation and proliferation. Mechanistically, acetyl-CoA synthesis was repressed by the transcription factors TEAD2 and E2A, previously unknown to control acetyl-CoA synthesis. Knockdown of TEAD2 and E2A restored acetyl-CoA levels and inhibited tumor growth. Our findings causally link transcriptional reprogramming of acetyl-CoA metabolism, dedifferentiation, and cancer.

INTRODUCTION

Acetyl-CoA is a central metabolite required for many physiological processes including histone and non-histone protein acetylation, metabolite acetylation, the TCA cycle, and *de novo* fatty acid synthesis. Acetyl-CoA is produced via multiple pathways including branched chain amino acid (BCAA) catabolism, fatty acid oxidation (FAO), pyruvate catabolism, ketolysis, and other minor biosynthesis pathways.[1]

Acetyl-CoA synthesis pathways are often up- or down-regulated in cancer, in a cancer type-dependent manner. BCAA catabolism is enhanced in pancreatic ductal adenocarcinoma (PDAC) but reduced in hepatocellular carcinoma (HCC).[2,3] Ovarian and breast cancer display increased expression of enzymes in FAO, whereas several other cancers, including lung cancer, clear cell renal cell carcinoma (ccRCC), and HCC, display reduced expression of FAO enzymes.[4–7] Pyruvate catabolism is suppressed in several cancers, including head and neck squamous cell carcinoma (HNSCC), ccRCC, and breast cancer.[8] Thus, individual acetyl-CoA synthesis pathways have been shown to be altered in cancer. As mentioned above, enzymes in BCAA catabolism or FAO can be reduced in HCC, likely to maintain BCAAs and acylcarnitine levels.[2,5] However, BCAA catabolism and FAO are also major acetyl-CoA biosynthesis pathways. Thus, alteration of these pathways could also impact acetyl-CoA levels. Despite the fact that acetyl-CoA is a key metabolite, it remains to be investigated whether global acetyl-CoA synthesis and cellular acetyl-CoA levels change in cancer cells. It is also unknown if acetyl-CoA impacts tumorigenesis beyond histone modification.

The liver is a major metabolic organ that controls carbohydrate, lipid, and amino acid metabolism. Hepatocytes, the primary cells of the liver, dedifferentiate during tumorigenesis and thereby cease to carry out many metabolic functions.[9–11]

Here, we sought to investigate cancer-associated reprogramming of acetyl-CoA metabolism and its role in tumorigenesis in HCC, the major subtype of liver cancer. We found that all acetyl-CoA biosynthetic pathways are transcriptionally

repressed in HCC, by TEAD2 and E2A, resulting in reduced acetylation of non-histone proteins and promotion of dedifferentiation/stemness and tumorigenesis. Thus, global repression of acetyl-CoA synthesis promotes oncogenicity via reduced protein acetylation.

RESULTS

Acetyl-CoA and non-histone protein acetylation are decreased in HCC

To investigate acetyl-CoA metabolism in HCC, we first examined acetyl-CoA levels and protein acetylation in HCC patients and an HCC mouse model. The HCC mouse model (hepatocyte-specific, *albumin-Cre* driven deletion of the tumor suppressors *Pten* and *Tsc1*, hereafter referred to as L-dKO) displayed aggressive, dedifferentiated liver tumors within 20 weeks of birth.[12–14] Surprisingly, acetyl-CoA levels were decreased in tumor tissue from HCC patients (Figure 1A) and L-dKO mice (Figure 1B), compared with control tissues. Consistent with the decrease in acetyl-CoA, total protein acetylation was significantly reduced in patient (Figure 1C) and L-dKO tumors (Figure 1D), as measured by immunoblotting tissue extracts with an antibody recognizing acetylated lysine. Immunohistochemistry on tissue of HCC patients and L-dKO mice confirmed that protein acetylation was strongly reduced in tumors compared with non-tumor areas (Figures 1E and 1F). Thus, acetyl-CoA levels and protein acetylation are decreased in HCC.

To quantify protein acetylation and to determine the identity of the proteins whose acetylation changes in tumors, we analyzed the acetylome and paired proteome of L-dKO tumors and control livers (Figure S1A). We quantified 1,271 acetylated peptides corresponding to 402 proteins, common to tumors and controls. After normalization of the acetylome to the matching proteome, 211 peptides from 158 proteins were hypo-acetylated, whereas only 63 peptides from 52 proteins were hyper-acetylated in tumors (Figures 1G–1I, S1B–S1D, S2A, and S2B). Among the proteins that were hypo-acetylated, most were metabolic enzymes involved in, for example, glycolysis, amino acid metabolism, the TCA cycle, and oxidative phosphorylation (OXPHOS) (Figures S1E and S1F). Acetylation can impact a protein's activity, specificity, localization, or stability (Figures 1I and S1C).[15–17] However, the effect of acetylation is unknown for most proteins, including those proteins whose acetylation was changed in tumors (Figures S2A and S2B). Our findings suggest that reduced cellular protein acetylation may broadly impact metabolism to promote oncogenicity.

We also quantified acetylation of 17 peptides from histones H2, H3, and H4. Two peptides were hypo-acetylated and two were hyper-acetylated, whereas the remaining 13 peptides were unchanged in tumors (Figure S2C). We next probed with antibodies that specifically recognize acetylated histones H3 and H4. There was little to no change in global acetylation of histones H3 and H4 in patients and L-dKO tumors (Figure S2D) compared with control livers. These findings suggest that specifically non-histone protein acetylation is decreased in tumors. The apparent lack of an effect on histone acetylation is likely due to the fact that lysine acetyltransferases (KATs) in the nucleus can use a local pool of acetyl-CoA derived from recycled acetate.[18] We note that the nuclear form of acetyl-CoA synthetase 2 (ACSS2, also known as AceCS1) and nuclear acetyl-CoA levels were unchanged in tumors, whereas the cytoplasmic form of ACSS2 and cytosolic and mitochondrial acetyl-CoA levels were decreased (Figures S2E and S2F).

Acetyl-CoA synthesis pathways are transcriptionally inhibited in HCC

To gain insight on the mechanism by which acetyl-CoA levels are decreased, we analyzed the transcriptome and proteome from both patient HCC needle biopsies[19] and L-dKO mouse tumors.[12] The HCC needle biopsies were paired with non-tumor liver biopsies from the same patient. Transcriptomic analysis was performed on 122 biopsies from 114 patients, of which a subset of 51 biopsies from 49 patients was subjected to proteomic analysis. The 122 biopsies and its subset included HCCs of different etiologies and aggressiveness (see STAR Methods). Samples from the L-dKO tumors were compared with liver samples from wild-type littermate controls.

Our omics analyses revealed transcriptional downregulation of all acetyl-CoA synthesis pathways (Figure 2A), including BCAA catabolism, FAO, pyruvate catabolism, and ketolysis. BCAA catabolism is a multi-step process that generates acetyl-CoA from the degradation of leucine, valine, and isoleucine.[20] mRNA and protein levels of BCAA catabolism enzymes were decreased in tumor tissue from both HCC patients (Figure 2B) and L-dKO mice (Figure 2C). This decrease in expression of BCAA catabolism enzymes was particularly pronounced in aggressive tumors, i.e., tumors classified as high grade in the Edmondson-Steiner clinical scale (Figure 2B). The loss of BCAA catabolism enzymes in tumors was confirmed by immunoblotting resected tumor tissue from HCC patients and L-dKO mice (Figures 2D and 2E).

FAO shares several enzymes with BCAA catabolism and also generates acetyl-CoA as a final product.[21] FAO-specific enzymes, like the FAO enzymes shared with BCAA catabolism, were decreased in tumors at the mRNA and protein levels (Figures 2B and 2C). Again, the extent of downregulation correlated with tumor severity as graded on the Edmondson-Steiner scale (Figure 2B). Loss of FAO enzymes was confirmed by immunoblotting (Figure 2D). Furthermore, acylcarnitine species, upstream metabolites in FAO, accumulated in L-dKO tumors compared with control livers. The observed accumulation of acylcarnitine species and depletion of FAO intermediate metabolites indicate that the FAO pathway was indeed inhibited (Figure 2F).

Pyruvate catabolism is the third major pathway of acetyl-CoA synthesis. Pyruvate, the final product of glycolysis, is converted to acetyl-CoA by the pyruvate dehydrogenase complex (PDC). Pyruvate dehydrogenase kinases (PDKs), of which PDK1 and PDK2 are the two major isoforms in liver,[22] phosphorylate and inhibit PDC to prevent pyruvate catabolism.[23] Specifically, PDKs phosphorylate pyruvate dehydrogenase E1 component subunit alpha (PDHA1) of PDC.[24] In patient samples, PDK1 and PDK2 expression and PDHA1 phosphorylation were increased in high Edmondson-Steiner grade tumors (Figure 2B). In L-dKO tumors, PDK1 expression and PDHA1 phosphorylation were increased, and PDC activity was decreased (Figures 2G and 2H). Thus, pyruvate catabolism is attenuated in HCC.

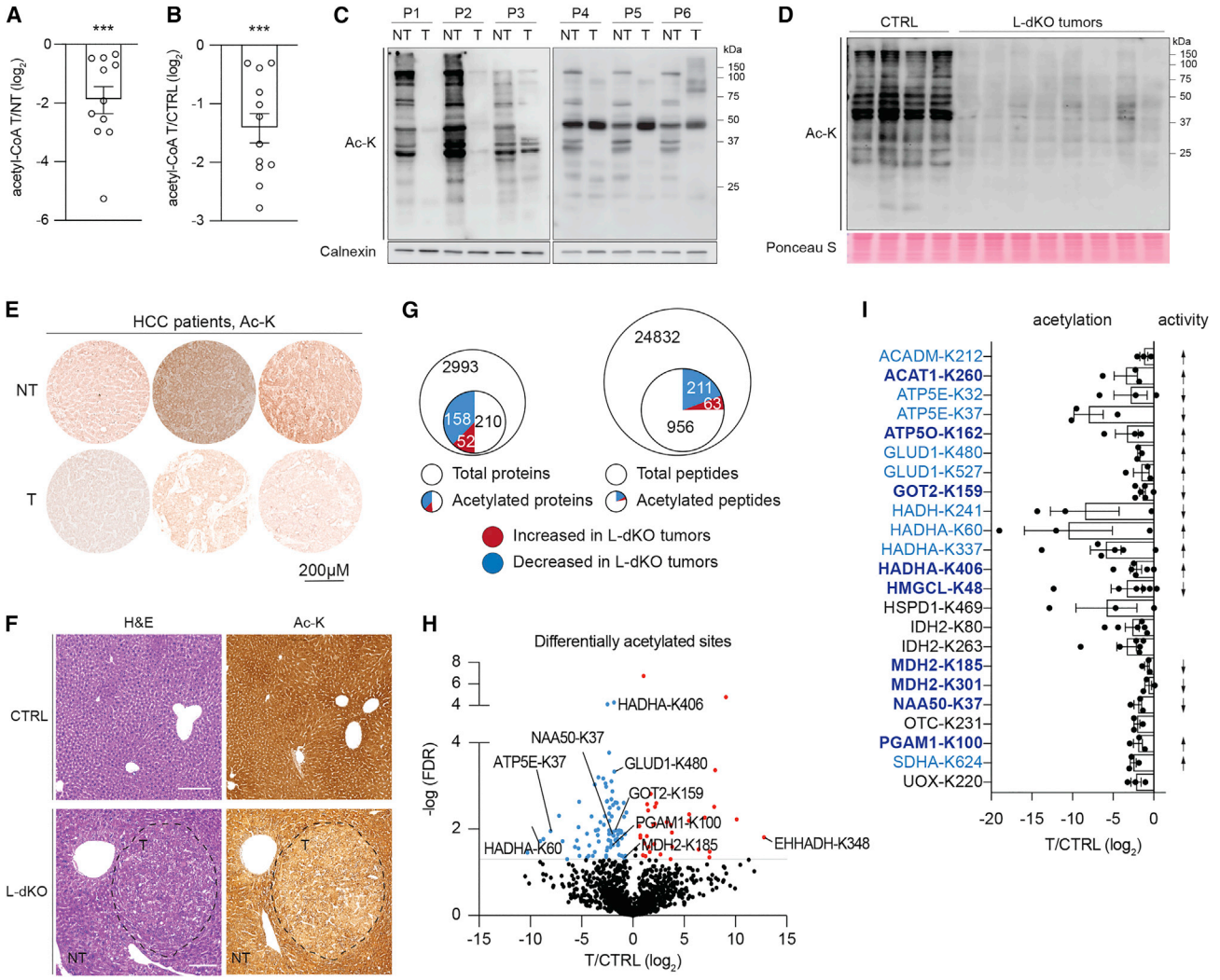

Figure 1. Acetyl-CoA and protein acetylation are decreased in HCC

(A) Acetyl-CoA levels in liver tumor tissue (T) of HCC patients compared with adjacent non-tumor tissue (NT). n = 11. Student's t test, *** $p < 0.001$.

(B) Acetyl-CoA levels in L-dKO tumors (T) compared with control liver tissue (CTRL). n = 12. Student's t test, *** $p < 0.001$.

(C) Immunoblots of liver tumor tissue (T) from HCC patients compared with adjacent non-tumor tissue (NT). Calnexin serves as a loading control. n = 6, protein acetylation on lysine residues (Ac-K).

(D) Immunoblots of L-dKO tumors compared with control liver tissue (CTRL). Ponceau S image serves as a loading control. n = 4 (CTRL) and 4 (two tumors per L-dKO mouse).

(E) Immunohistochemistry analyses of tumor tissue (T) from HCC patients compared with adjacent normal tissue (NT). Scale bars, 200 μm.

(F) Immunohistochemistry analyses of L-dKO liver compared with control liver (CTRL). Black boundaries in L-dKO indicate a tumor (T). Outside of the black boundaries indicates a non-tumor (NT). Scale bars, 200 μm.

(G) Number of proteins, peptides, and acetylated peptides were quantified in tumors and control tissue. Numbers in a big circle indicate total protein and peptide. Numbers in the inner circle indicate acetylated proteins and peptides.

(H) Volcano plot of the $-\log_{10}$ false discovery rate (FDR) against the $\log_2$ fold change of the differentially regulated acetylation sites in tumors compared with control tissue. Acetylation is normalized to protein expression. FDR < 0.05.

(I) Hypo-acetylated sites (Function of acetylation is studied. Acetylation site is either reported or unknown) in tumors compared with controls (less than -0.5 $\log_2$-fold change at least in two experiments). Acetylation is normalized to protein expression. Functional prediction of hypo-acetylated proteins in tumors based on previous publications. Acetylation of lysine residues in bold blue is functionally known. Lysine residues in sky blue are functionally unknown, but acetylation of those proteins is studied.

We also investigated whether other, minor acetyl-CoA synthesis pathways such as ketolysis, acetaldehyde oxidation, acetate metabolism, and ATP-citrate synthase lyase (ACLY) are altered in HCC. Ketolysis breaks down the ketone body β-hydroxybutyrate (β-HB) to produce acetyl-CoA in mitochondria.[25] Two of the three enzymes in the ketolysis pathway were decreased in both patient and mouse tumors, as determined by transcriptomic, proteomic, and immunoblot analyses (Figures 2B–2D). Loss of

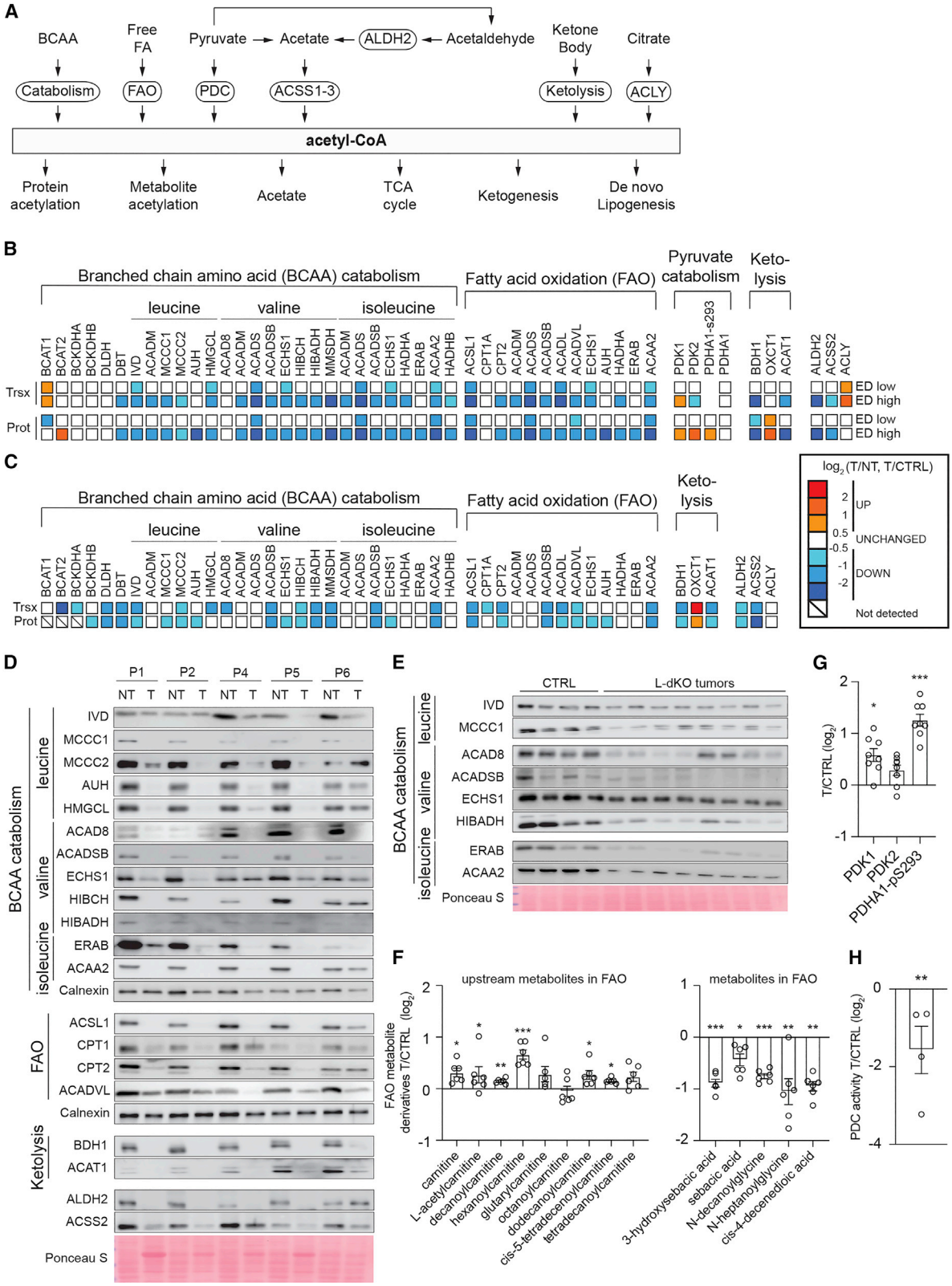

(legend on next page)

enzyme expression was more prominent in high Edmondson-Steiner grade tumors compared with low Edmondson-Steiner grade tumors (Figure 2B). Acetaldehyde is converted to acetate by aldehyde dehydrogenase 2 (ALDH2),[26] and acetate is converted to acetyl-CoA by ACSS2 .[27,28] Expression of both ALDH2 and ACSS2 was significantly decreased in patient (Figure 2B) and L-dKO (Figure 2C) tumors, confirming previous findings in human, HBV-associated HCC.[29,30] The above findings that major and minor acetyl-CoA biosynthesis pathways are transcriptionally suppressed, particularly in aggressive tumors, suggest that reduced acetyl-CoA levels may play a role in HCC. We note that ACLY, which catalyzes the cleavage of mitochondria-derived citrate to produce acetyl-CoA and oxaloacetate, was unchanged in patient and mouse tumors (Figures 2B and 2C). We also note that there are conflicting views on the role of ACSS2 in HCC.[30–33]

TEAD2 and E2A inhibit acetyl-CoA synthesis genes

We next sought to determine the mechanism of the transcriptional inhibition of acetyl-CoA synthesis pathways in tumors. It has been reported that knockdown or pharmacological inhibition of peroxisome proliferator-activated receptor alpha (PPARα) reduced expression of some BCAA catabolism genes in human hepatoblastoma HepG2 cells.[2] In addition, PPARα induced expression of *CPT2* (encoding an enzyme involved in FAO) in HepG2 cells.[34] We observed decreased *PPARα* expression in tumors of HCC patients and L-dKO mice (Figures S3A and S3B). To determine whether PPARα broadly regulates BCAA catabolism, FAO, and ultimately protein acetylation, we knocked down and overexpressed PPARα in cells. CPT2 expression was increased and decreased upon overexpression and knockdown of PPARα, respectively (Figures S3C and S3D), confirming that PPARα controls CPT2 expression. However, there was little to no effect on expression of other acetyl-CoA synthesis genes or on protein acetylation (Figures S3C and S3D). Thus, we speculated that transcription factors other than PPARα mediate global regulation of acetyl-CoA metabolism.

Examination of the transcriptomes of patient tumors revealed that expression of acetyl-CoA synthesis genes inversely correlated with expression of the two transcription factors transcriptional enhanced associate domain 2 (TEAD2) and transcription factor E2-alpha (E2A, also known as TCF3) (Figures S3E and S3F). Targeted analysis confirmed increased expression of TEAD2 and E2A in tumors, in HCC patients and L-dKO mice (Figures 3A–3D and S3G). JASPAR analysis revealed TEAD2 and E2A binding motifs in the promoter regions of eight and fifteen acetyl-CoA synthesis genes, respectively (Figures S3H–S3K). Seven of these genes have both motifs. TEAD2 and E2A can act as transcriptional repressors,[35–37] consistent with the inverse correlation in expression of acetyl-CoA synthesis genes and the two transcription factors (Figures S3E and S3F). Altogether, the above suggests that TEAD2 and E2A impact the expression of acetyl-CoA synthesis genes in tumors.

To investigate the inhibition of acetyl-CoA synthesis genes by TEAD2 and E2A, we performed knockdown or overexpression studies *in vitro* using human HCC SNU449 cells and L-dKO mouse tumor CB1 cells,[14] both of which display reduced expression of acetyl-CoA synthesis genes. Stable knockdown of *TEAD2* with short hairpin RNAs (shRNAs) restored expression of acetyl-CoA synthesis genes (Figures 3E, S4A, and S4B). Furthermore, acetyl-CoA levels and total protein acetylation increased upon *TEAD2* knockdown (Figures 3F, 3G, and S4C). Conversely, enhanced expression of TEAD2 in SNU449 and CB1 cells reduced expression of acetyl-CoA synthesis enzymes (Figures 3H, S4D, and S4E), levels of acetyl-CoA (Figure 3J), and global protein acetylation (Figures 3I and S4F). Stable knockdown of the three *TEADs* (*TEAD1*, *3*, and *4*) other than *TEAD2* did not affect expression of acetyl-CoA synthesis enzymes or global protein acetylation (Figures S4G and S4H). We note that expression of the other *TEADs* was not changed in L-dKO tumors (Figure S4I). Thus, TEAD2 represses expression of acetyl-CoA synthesis genes.

TEADs (TEAD1-4) often activate gene expression in concert with the transcription factors yes-associated protein (YAP) and transcriptional coactivator with PDZ-binding motif (TAZ). Conversely, vestigial-like proteins (VGLL1-4) compete with YAP and TAZ for TEAD binding, resulting in inhibition of YAP/TAZ.[38] Thus, we investigated whether YAP/TAZ or VGLLs mediate TEAD2's repression of acetyl-CoA synthesis genes. We did not observe altered expression of *YAP*, *TAZ*, and *VGLLs* in HCC patients other than a mild decrease of *VGLL1* and increase of *VGLL3* expression (Figure S4J). mRNA levels of *Vgll4* were unchanged in L-dKO tumors, whereas expression of *Yap*

Figure 2. Acetyl-CoA synthesis pathways are decreased in HCC

(A) Overview of acetyl-CoA metabolism.

(B) Summary of mRNA (transcriptome, trsx) and protein (proteome, prot) expression changes in branched chain amino acid (BCAA) catabolism, fatty acid oxidation (FAO), pyruvate catabolism, ketolysis, and acetyl-CoA synthesis enzymes of HCC patient biopsies. mRNA (transcriptome, trsx) and protein (proteome, prot) abundance in tumors (T) compared with adjacent non-tumor liver tissue (NT), represented in $\log_2$ based color code. Tumor aggressiveness is indicated by Edmondson-Steiner grade low (EDL, grade I and II) and high (EDH, grade III and IV). n = 73 (EDL) and 49 (EDH) for mRNA level, n = 30 (EDL) and 21 (EDH) for protein level and PDHA1-s293 phosphorylation.

(C) Summary of mRNA and protein expression changes in BCAA catabolism, FAO, ketolysis, acetyl-CoA synthesis enzymes in L-dKO tumors. mRNA and protein abundance in tumors (T) compared with control liver tissue (CTRL), represented in $\log_2$-based color code. n = 6 (CTRL) and 4 (three tumors per L-dKO mouse).

(D) Immunoblots of liver tumor tissue (T) from HCC patients compared with adjacent non-tumor tissue (NT). Calnexin and Ponceau S serve as a loading control. n = 5.

(E) Immunoblots of L-dKO tumors compared with control liver tissue (CTRL). Ponceau S image serves as a loading control. n = 4 (CTRL) and 4 (two tumors per L-dKO mouse).

(F) Non-targeted metabolomic analysis of L-dKO tumors (T) compared with control liver tissue (CTRL). n = 5 (CTRL) and 6 (L-dKO tumors). Multiple t test, * $p < 0.05$, ** $p < 0.01$, *** $p < 0.001$.

(G) Quantification of PDK1, PDK2, PDHA1, and PDHA1-pS293 of tumors of L-dKO (T) compared with control liver tissue (CTRL). Phosphorylation is normalized to total protein.

(H) Enzyme activity of PDC in tumors of L-dKO (T) compared with control liver tissue (CTRL). n = 4. Student's t test, ** $p < 0.01$.

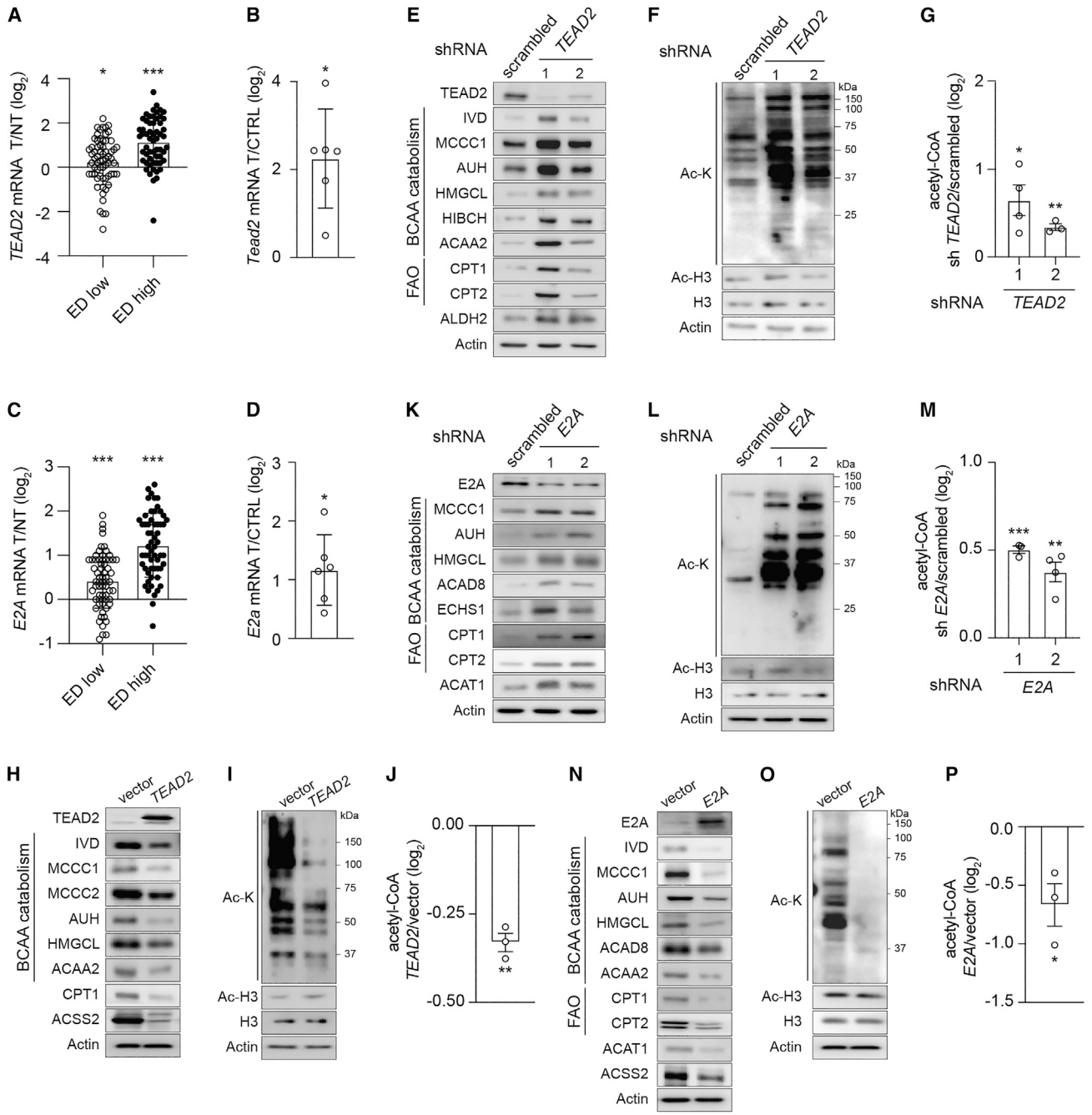

Figure 3. TEAD2 and E2A regulate acetyl-CoA synthesis and protein acetylation

(A) *TEAD2* mRNA levels in liver tumor tissue (T) from HCC patients compared with adjacent non-tumor tissue (NT). n = 73 (ED low) and 49 (ED high), Multiple t test, * $p < 0.05$, *** $p < 0.001$.

(B) *Tead2* mRNA levels in L-dKO tumors (T) compared with control liver tissue (CTRL). n = 6. Student's t test, * $p < 0.05$.

(C) *E2A* mRNA levels in liver tumor tissue (T) from HCC patients compared with adjacent non-tumor tissue (NT). n = 73 (ED low) and 49 (ED high), Multiple t test, *** $p < 0.001$.

(D) *E2a* mRNA levels in L-dKO tumors (T) compared with control liver tissue (CTRL). n = 6. Student's t test, * $p < 0.05$.

(E and F) Immunoblots upon control (scrambled) and *TEAD2* knockdown in SNU449 cells. Actin serves as a loading control. Protein acetylation on lysine residues (Ac-K).

(G) Acetyl-CoA levels upon *TEAD2* knockdown compared with control SNU449 cells (scrambled). N = 4 (scrambled) and 3–4 (*TEAD2* knockdown). Multiple t test, * $p < 0.05$, ** $p < 0.01$.

(H and I) Immunoblots upon control (vector) and TEAD2 overexpression in SNU449 cells.

(legend continued on next page)

and *Taz* was decreased and increased, respectively (Figure S4K). We did not observe changes in YAP phosphorylation or VGLL4 expression upon knockdown or overexpression of *TEAD2* in SNU449 cells (Figure S4L). Furthermore, expression of acetyl-CoA synthesis genes and global protein acetylation were unchanged upon treatment with verteporfin, an inhibitor of YAP-TEAD interaction (Figure S4M). Thus, repression of acetyl-CoA synthesis genes by TEAD2 is independent of YAP/TAZ and VGLLs.

Similar to the effect of TEAD2 on acetyl-CoA synthesis and protein acetylation, stable knockdown of *E2A* with shRNAs restored expression of acetyl-CoA synthesis genes (Figures 3K, S5A, and S5B). Furthermore, acetyl-CoA levels and total protein acetylation increased upon *E2A* knockdown (Figures 3L, 3M, and S5C). Conversely, enhanced expression of E2A in SNU449 and CB1 cells reduced expression of acetyl-CoA synthesis genes (Figures 3N, S5D, and S5E), levels of acetyl-CoA (Figure 3P), and global protein acetylation (Figures 3O and S5F). Thus, E2A, like TEAD2, negatively controls acetyl-CoA synthesis genes.

We next assayed the effect of TEAD2 and E2A overexpression on promoter activity of selected acetyl-CoA synthesis genes, using luciferase reporter constructs containing approximately 1,000 bp promoter fragments of such genes, in SNU449 cells. Overexpression of E2A, but not of TEAD2, repressed the promoter of the acetyl-CoA synthesis gene *ACAD8* (Figure S5G) that is presumably a target only of E2A (Figure S3F). Overexpression of either E2A or TEAD2 repressed the promoters of the acetyl-CoA synthesis genes *ACAA2*, *CPT2*, and *IVD* that contain both E2A and TEAD2 binding motifs (Figure S5G). These findings provide further evidence of transcriptional repression of acetyl-CoA synthesis genes by TEAD2 and E2A and validate the above correlation and JASPER analyses. We note that we did not obtain a reporter construct containing the promoter region of the single, TEAD2-specific acetyl-CoA synthesis gene *ALDH2*.

Consistent with the above observation that histone acetylation was unchanged in tumors (Figure S2D), changes in TEAD2 and E2A expression had no effect on histone H3 acetylation (Figures 3F, 3I, 3L, 3O, S4C, S4F, S5C, and S5F). Our findings suggest that TEAD2 and E2A inhibit acetyl-CoA synthesis genes and thereby reduce acetyl-CoA levels and acetylation of non-histone proteins.

TEAD2 and E2A promote cell proliferation

To evaluate the importance of TEAD2 and E2A in tumorigenesis, we investigated whether TEAD2 and E2A affect HCC cell proliferation. Indeed, *TEAD2* or *E2A* knockdown reduced clonogenic proliferation in SNU449 and CB1 cells (Figures 4A, 4B, S5H, and S5I). Conversely, overexpression of TEAD2 or E2A enhanced clonogenic proliferation (Figures 4C, 4D, S5J, and S5K). These findings suggest that TEAD2 and E2A promote cancer cell proliferation.

To investigate whether the effect of overexpressing TEAD2 and E2A is due to reduced levels of acetyl-CoA and protein acetylation, we restored acetyl-CoA levels by providing acetyl-CoA replenishing reagent (ARR). ARR is a mixture of keto acids (which are substrates for BCAA catabolism), DCA (which activates pyruvate catabolism), and aceto-acetate (which is a substrate for ketolysis). Exogenously added ARR increased cellular acetyl-CoA and protein acetylation levels (Figures 4E–4H). ARR treatment also reduced clonogenic proliferation of TEAD2 or E2A overexpressing cells without affecting proliferation of control cells (Figures 4I and 4J). To investigate further the effect of acetyl-CoA on proliferation, we manipulated acetyl-CoA levels by overexpressing ACSS2 or knocking down *PDK1/2* in HCC cells. Consistent with decreased proliferation upon ARR treatment, protein acetylation was increased and clonogenic proliferation was reduced upon ACSS2 overexpression or *PDK1/2* knockdown (Figure S6). Altogether, these findings suggest that TEAD2 and E2A promote cell proliferation by suppressing expression of acetyl-CoA synthesis pathways, ultimately reducing acetyl-CoA levels.

TEAD2 and E2A promote dedifferentiation

To evaluate further the importance of TEAD2 and E2A in tumorigenesis, we investigated their effect on dedifferentiation/stemness. Upon combined overexpression of TEAD2 and E2A, we observed enhanced hepatosphere formation in SNU449 cells (Figures 5A and 5B). This observation led us to examine whether combined overexpression of TEAD2 and E2A affects expression of the dedifferentiation/stemness makers oncofetal Sal-like protein 4 (SALL4)[39] and pluripotency transcription factors octamer-binding protein 4 (OCT4), NANOG, and SOX2.[10] Expression of SALL4, OCT4, NANOG, and SOX2 was increased upon TEAD2 and E2A overexpression, in SNU449 cells (Figures 5C and 5D). In addition, cancer stem cell markers, including epithelial cell adhesion molecule (EpCAM) and CD44, and the epithelial-mesenchymal transition (EMT) marker neuronal cadherin (N-cadherin) were increased upon combined TEAD2 and E2A overexpression. Conversely, hepatocyte differentiation markers, including albumin and cytochrome P450 monooxygenases (CYPs), were downregulated upon combined TEAD2 and E2A overexpression (Figure 5D). We note that overexpression of E2A alone also enhanced hepatosphere formation and dedifferentiation/stemness (Figures S7A–S7C), whereas overexpression of TEAD2 alone had no effect on hepatosphere formation. Combined overexpression of TEAD2 and E2A increased expression of EMT markers in SNU449 cells compared with overexpression of E2A alone (Figure S7D). Simultaneous overexpression of TEAD2 and E2A enhanced hepatosphere formation in Huh1 and non-cancerous mouse AML12 hepatocytes (Figures S7E–S7H), whereas overexpression of TEAD2 or E2A alone had no effect. Combined overexpression of TEAD2 and E2A increased

(J) Acetyl-CoA levels upon TEAD2 overexpression compared with control SNU449 cells (vector). N = 3. Student's t test, ** $p < 0.01$.
(K and L) Immunoblots upon control (scrambled) and *E2A* knockdown in SNU449 cells.
(M) Acetyl-CoA levels upon *E2A* knockdown compared with control SNU449 cells (scrambled). N = 4 (scrambled) and 2–4 (*E2A* knockdown). Multiple t test, ** $p < 0.01$, *** $p < 0.001$.
(N and O) Immunoblots of control (vector) and E2A overexpressing SNU449 cells.
(P) Acetyl-CoA levels upon E2A overexpression compared with control SNU449 cells (vector). N = 3. Student's t test, * $p < 0.05$.

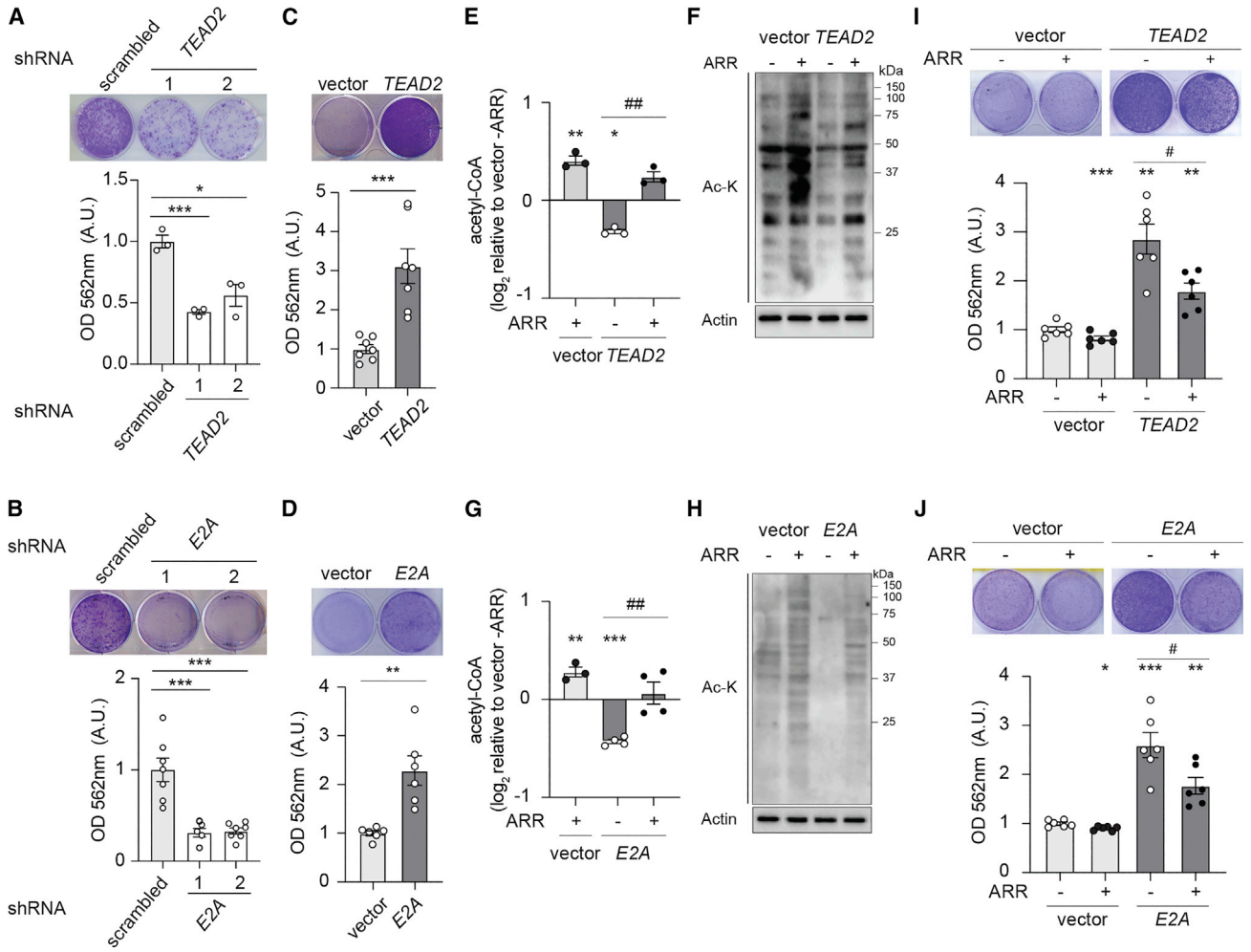

Figure 4. TEAD2 and E2A regulate clonogenic proliferation via reduction of acetyl-CoA levels

(A) Clonogenic growth assay upon control (scrambled) and *TEAD2* knockdown in SNU449 cells. N = 3. Multiple t test, * $p < 0.05$, *** $p < 0.001$.

(B) Clonogenic growth assay upon control (scrambled) and *E2A* knockdown in SNU449 cells. N = 7 (scrambled) and 5–7 (*E2A* knockdown). Multiple t test, *** $p < 0.001$.

(C) Clonogenic growth assay upon control (vector) and TEAD2 overexpression in SNU449 cells. N = 7. Student's t test, *** $p < 0.001$.

(D) Clonogenic growth assay of control (vector) and E2A overexpressing SNU449 cells. N = 6. Student's t test, ** $p < 0.01$.

(E) Acetyl-CoA levels upon TEAD2 overexpression compared with control (vector) SNU449 cells with or without acetyl-CoA replenishing reagents (ARR). N = 3. Multiple t test, * $p < 0.05$, ** $p < 0.01$, ## $p < 0.01$.

(F) Immunoblots upon control (vector) and TEAD2 overexpression in SNU449 cells with or without ARR. Actin serves as a loading control. protein acetylation on lysine residues (Ac-K).

(G) Acetyl-CoA levels upon E2A overexpression in SNU449 cells compared with control (vector) with or without ARR. N = 3–4. Multiple t test, ** $p < 0.01$, *** $p < 0.001$, ## $p < 0.01$.

(H) Immunoblots upon control (vector) and E2A overexpression in SNU449 cells with or without ARR.

(I) Clonogenic growth assay upon control (vector) and TEAD2 overexpression in SNU449 cells with or without ARR. N = 6. Multiple t test, ** $p < 0.01$, *** $p < 0.001$, # $p < 0.05$.

(J) Clonogenic growth assay of control (vector) and E2A overexpressing SNU449 cells with or without ARR. N = 6. Multiple t test, * $p < 0.05$, ** $p < 0.01$, *** $p < 0.001$, # $p < 0.05$.

expression of EpCAM, N-cadherin, OCT4, and SOX2 in Huh1 cells compared with overexpression of TEAD2 alone (Figure S7I). Thus, TEAD2 and E2A synergistically promote hepatosphere formation and dedifferentiation/stemness in several HCC cell lines.

In an inverse approach, we investigated whether cancer cells that have cancer stem cell characteristics (cancer stem-like cells, CSCs) display increased expression of TEAD2 and E2A. We isolated cells with the highest and lowest expression of CD44 from a culture of CB1 cells, by flow cytometry (Figure 5E). CD44, a plasma membrane receptor, is highly expressed in stem cells, including liver CSCs.[40–43] CD44 high cells displayed higher levels of TEAD2, E2A, and dedifferentiation markers, compared with CD44 low cells. In addition, global protein acetylation and expression of acetyl-CoA synthesis genes were reduced in

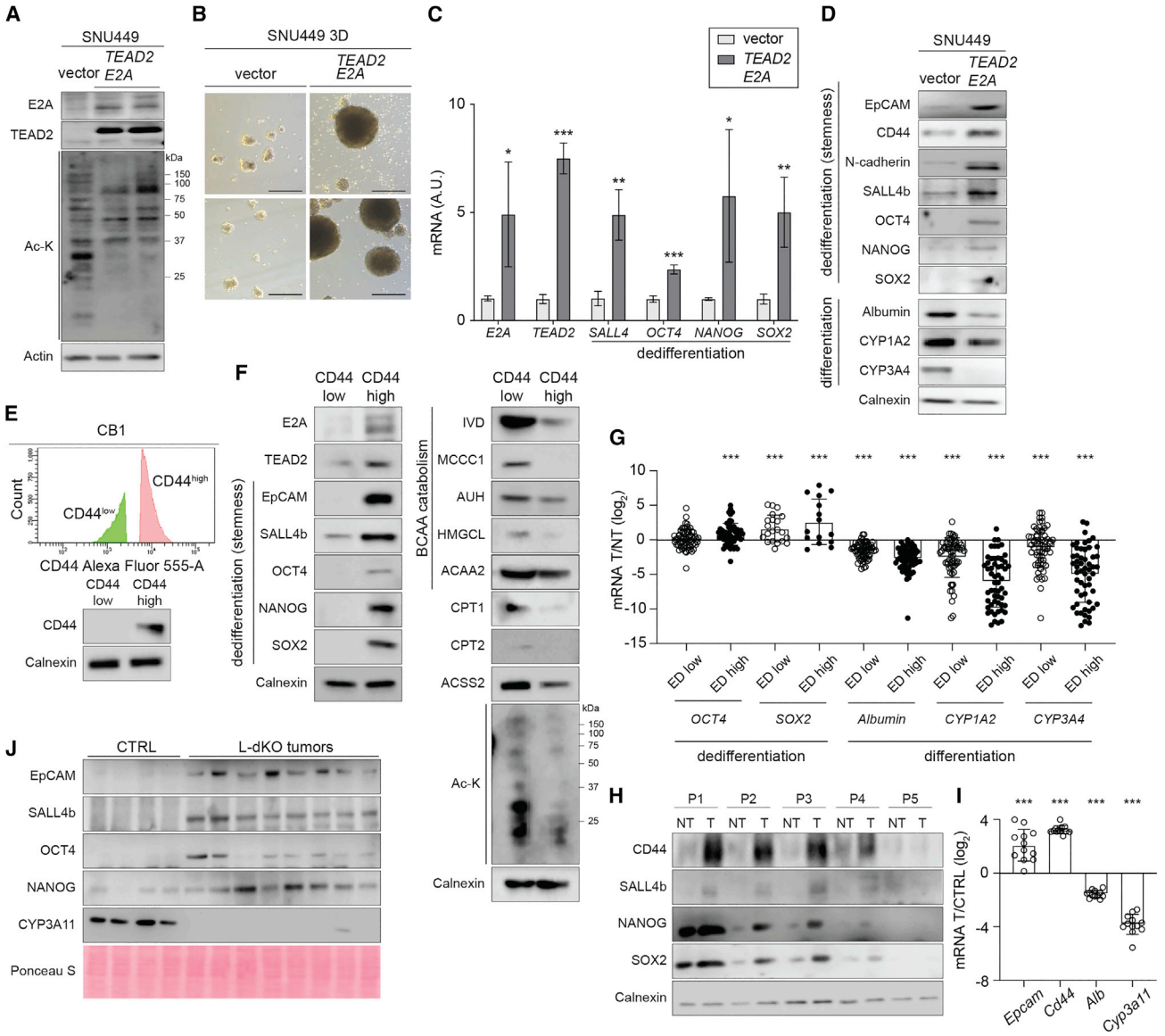

Figure 5. TEAD2 and E2A promote dedifferentiation

(A) Immunoblots of control SNU449 cells (vector) and SNU449 cells overexpressing TEAD2 and E2A. Actin serves as a loading control. protein acetylation on lysine residues (Ac-K).

(B) Bright field images of 3D- long term cultured SNU449 control cells (vector) and overexpressing TEAD2 and E2A. Scale bars, 100 μm.

(C) mRNA levels of *E2A*, *TEAD2*, and pluripotency transcription factors in control SNU449 cells (vector) and SNU449 cells overexpressing TEAD2 and E2A. N = 3–4. Multiple t test, * $p < 0.05$, ** $p < 0.01$, *** $p < 0.001$.

(D) Immunoblots of control SNU449 cells (vector) and SNU449 cells overexpressing TEAD2 and E2A. Calnexin serves as a loading control.

(E) Top 25% of CD44 high or low subpopulations of CB1 cells isolated by fluorescence-activated cell sorting (FACS). Cells were labeled with Alexa 555 conjugated anti-CD44 antibody. Immunoblots of CD44 low and CD44 high CB1 cells were used to validate FACS.

(F) Immunoblots of CD44 low and CD44 high CB1 cells.

(G) mRNA levels of *OCT4*, *SOX2*, *Albumin*, *CYP1A2*, and *CYP3A4* in liver tumor tissue (T) from HCC patients compared with adjacent non-tumor tissue (NT). n = 73 (ED low) and 49 (ED high). Multiple t test, *** $p < 0.001$.

(H) Immunoblots of liver tumor tissue (T) from HCC patients compared with adjacent non-tumor tissue (NT). n = 5.

(I) mRNA levels of *Epcam*, *Cd44*, *Albumin*, and *Cyp3a11* in liver tumors (T) from L-dKO compared with control livers (CTRL). n = 6 (pooled CTRL) and 4 (three tumors per L-dKO mouse). Student's t tests, *** $p < 0.001$.

(J) Immunoblots of L-dKO tumors compared with control livers (CTRL). n = 4 (CTRL and two tumors per L-dKO mouse). Ponceau S serves as a loading control.

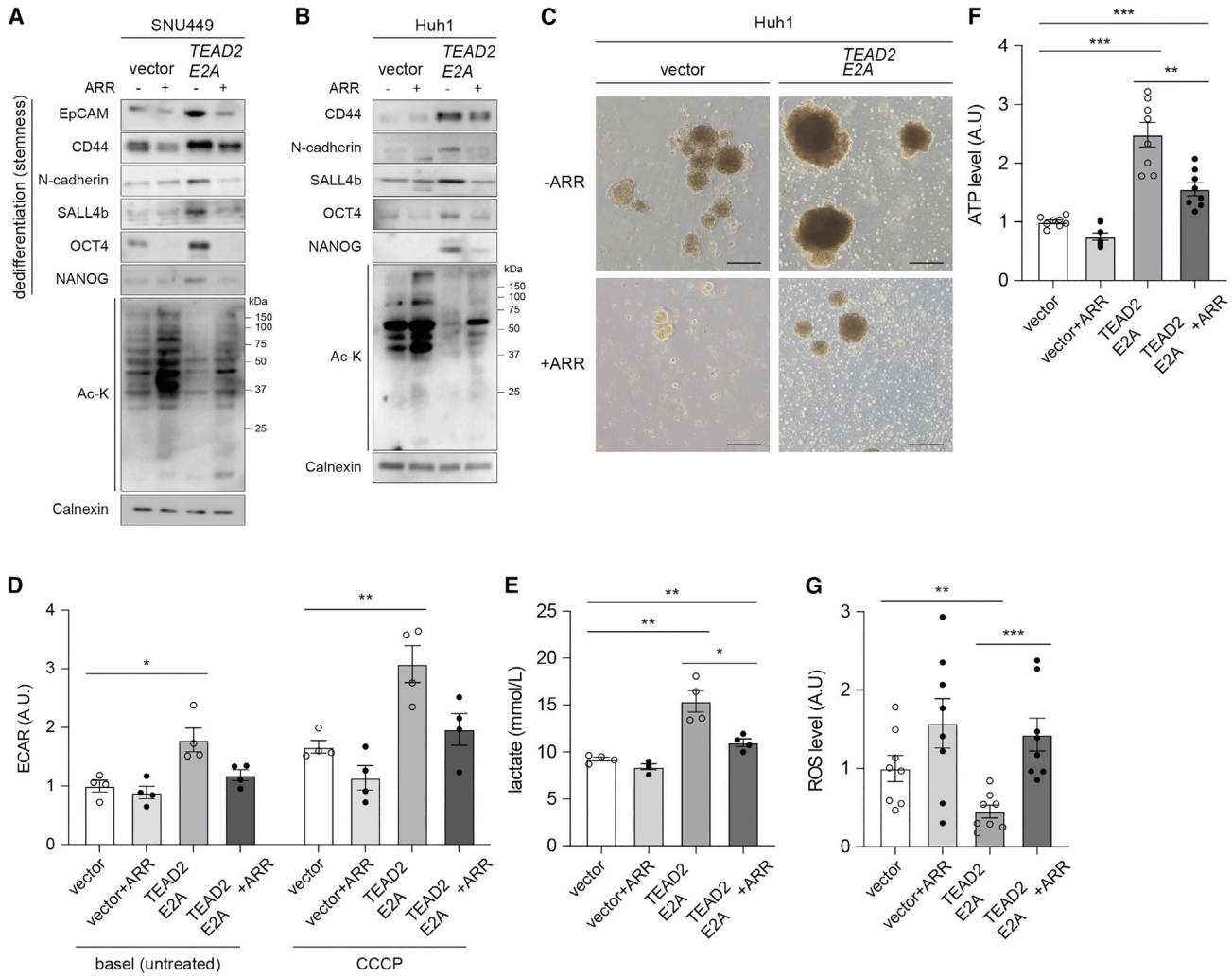

Figure 6. TEAD2 and E2A promote dedifferentiation and enhance metabolic fitness via reduction of acetyl-CoA levels

(A) Immunoblots of control SNU449 cells (vector) and SNU449 cells overexpressing TEAD2 and E2A with or without acetyl-CoA replenishing reagents (ARR) treatment for 2 days. Calnexin serves as a loading control. Protein acetylation on lysine residues (Ac-K).

(B) Immunoblots of control Huh1 cells (vector) and Huh1 cells overexpressing TEAD2 and E2A with or without ARR treatment for 2 days.

(C) Bright field images of Huh1 control cells (vector) and overexpressing TEAD2 and E2A in 3D culture with or without ARR treatment for one week. Scale bars, 100 μm.

(D–G) ECAR (D), extracellular lactate levels (E), ATP levels (F), and ROS levels (G) in control SNU449 cells (vector) and SNU449 cells overexpressing TEAD2 and E2A with or without acetyl-CoA replenishing reagents (ARR) treatment. Carbonyl cyanidem-chlorophenylhydrazone (CCCP) is used to stimulate maximal respiratory capacity by uncoupling proton pumping. N = 4–8. Multiple t test, * $p < 0.05$, ** $p < 0.01$, *** $p < 0.001$.

CD44 high cells (Figure 5F). Consistent with the above effects of TEAD2 and E2A in cell lines, we also observed increased expression of pluripotency transcription factors and decreased expression of hepatocyte differentiation markers in tumors of HCC patients and L-dKO mice (Figures 5G–5J). These findings provide further evidence that TEAD2 and E2A promote stemness in cancer.

Acetyl-CoA and protein acetylation inhibit dedifferentiation

We next investigated whether increased stemness upon overexpression of TEAD2 and E2A is due to decreased levels of acetyl-CoA and protein acetylation. Indeed, restoration of acetyl-CoA levels, by supplementing the growth medium with ARR, decreased expression of dedifferentiation genes, including pluripotency transcription factors and cancer stem cell markers (Figures 6A–6C and S8A–S8D). Thus, TEAD2 and E2A promote dedifferentiation/stemness and proliferation via reduction of acetyl-CoA levels. To determine whether the effect of decreased acetyl-CoA levels on dedifferentiation may be due to hypo-acetylation of pluripotency factors, we separately immunoprecipitated total acetylated proteins, OCT4, and SOX2 from TEAD2 and E2A overexpressing SNU449 cells and L-dKO tumors. OCT4 and SOX2 displayed reduced acetylation in TEAD2 and

E2A overexpressing SNU449 cells (Figures S8E and S8F) and L-dKO tumors (Figures S8G and S8H). This is consistent with studies in ES cells which found that deacetylation of OCT4 and SOX2 maintains pluripotency.[44,45] Altogether, the above suggests that dedifferentiation upon decreased acetyl-CoA levels is due to hypo-acetylation of pluripotency factors.

Next, we investigated whether the observed hypo-acetylation of metabolic enzymes contributes to tumorigenesis. TEAD2 and E2A overexpression enhanced glycolytic activity and ATP levels and decreased ROS levels, all of which were reversed upon ARR treatment (Figures 6D–6G). Thus, decreased acetyl-CoA levels may promote tumorigenicity by reducing acetylation of pluripotency transcription factors and metabolic enzymes (Figures 1I, 6, S1E, S1F, S2B, S7, and S8).

TEAD2 and E2A promote tumor growth and correlate with poor survival

To evaluate the effects of TEAD2 and E2A on tumor growth, we performed subcutaneous xenograft experiments with liver cancer cells (Huh7) in which both *TEAD2* and *E2A* were knocked down. *TEAD2* and *E2A* double-knockdown cells failed to form tumors, compared with control Huh7 cells (Figures 7A–7D). Thus, TEAD2 and E2A are important for tumor growth *in vivo* and, as described above, for proliferation and stemness *in vitro*.

As shown above, TEAD2 and E2A negatively regulate acetyl-CoA synthesis and thereby promote cell proliferation and stemness, leading to tumorigenesis. We next asked whether TEAD2 and E2A expression correlates with survival of HCC patients. Based on data from the The Cancer Genome Atlas (TCGA), TEAD2 and E2A expressions negatively correlate with overall survival (OS) and progression free survival (PFS) of HCC patients. Conversely, expression of acetyl-CoA synthesis genes positively correlates with OS and PFS (Figure 7E). These correlations further support the notion that TEAD2 and E2A promote tumorigenesis via inhibition of acetyl-CoA synthesis.

Do our findings in HCC apply to other cancers? Examination of TCGA data revealed that high TEAD2 and E2A expressions negatively correlate with OS and PFS also in ccRCC, pancreas adenocarcinoma, lung squamous cell carcinoma (LSCC), and prostate adenocarcinoma (Figures S9A–S9D). Furthermore, expression of acetyl-CoA synthesis genes positively correlates with OS and PFS in these cancers (Figures S9A–S9D). We confirmed that global protein acetylation is reduced in these cancers (Figures S9E–S9H). Thus, our findings appear to apply to tumors of other origin, suggesting a general importance of reprogramming of acetyl-CoA metabolism in tumorigenesis.

DISCUSSION

We show that transcriptional reprogramming of acetyl-CoA metabolism by TEAD2 and E2A promotes HCC. More specifically, acetyl-CoA levels and non-histone protein acetylation are decreased in HCC due to TEAD2- and E2A-mediated repression of acetyl-CoA synthesis genes. This in turn leads to dedifferentiation, proliferation, and tumor growth. The proteins that promote tumorigenesis when de-acetylated are likely metabolic enzymes and pluripotency transcription factors, including OCT4 and SOX2.

How do low acetyl-CoA levels and hypo-acetylation of proteins lead to cancer? First, previous studies in ES cells suggest that pluripotency transcription factors, including OCT4 and SOX2, are nuclear and transcriptionally active only when deacetylated. Conversely, increased cellular acetylation leads to increased proteasomal degradation of SOX2.[44,46] Thus, hypo-acetylation of pluripotency transcription factors may promote dedifferentiation and thereby maintain CSCs. We observed hypo-acetylation of OCT4 and SOX2 and nuclear localization of SOX2 in TEAD2 and E2A overexpressing SNU449 cells and L-dKO tumors (Figures S8E–S8H). Second, key enzymes in metabolic pathways, including glycolysis/gluconeogenesis, TCA cycle, and urea cycle, are acetylated.[47] Our acetylome analysis revealed that enzymes in glycolysis/gluconeogenesis, the TCA cycle, amino acid metabolism, ketone body metabolism, FAO, and OXPHOS are hypo-acetylated in liver tumors (Figures S1E, S1F, and S2B). Hypo-acetylation of succinate dehydrogenase flavoprotein subunit (SDHA), glutamate dehydrogenase 1 (GLUD1), malate dehydrogenase 2 (MDH2), and ATP synthase subunit O (ATP5O) can increase TCA cycle activity and OXPHOS.[47–50] In addition, hypo-acetylation of phosphoglycerate mutase 1 (PGAM1) can enhance enzyme activity and thereby promote glycolysis.[51] Reduced enzyme activity of hypo-acetylated hydromethylglutaryl-CoA lyase (HMGCL) and hydroxyacyl-CoA dehydrogenase (HADH) can further inhibit leucine catabolism and FAO[52,53] (Figure 1I). Furthermore, we observed that TEAD2 and E2A overexpressing cells have higher glycolytic activity and ATP levels, and lower ROS levels, compared with control cells (Figures 6D–6G). These observations are in agreement with reports that over half of all mitochondrial proteins are acetylated, and hypo-acetylation of metabolic enzymes (e.g., by SIRT3 overexpression) promotes cell proliferation and enhances ATP generation, glucose uptake, MNSOD activity, and lactate production.[54,55] In addition, it is reported that knockdown of *TEAD2* in ovarian serous carcinoma (OSC) induces ferroptosis by increasing ROS.[56] We note that metabolic fitness is reduced in TEAD2 and E2A overexpressing cells upon ARR treatment (Figures 6D–6G). Thus, low acetyl-CoA levels may promote tumorigenesis via hypo-acetylation of pluripotency factors and metabolic enzymes.

Altered histone acetylation and increased expression of histone deacetylases (HDACs) have been reported in many cancer types.[57,58] This led to the development and approval of pan-HDAC inhibitors (HDIs) for the treatment of T cell lymphomas and recurrent multiple myeloma.[59] However, HDIs have shown limited efficacy against solid tumors.[60] Our findings suggest that reduced acetyl-CoA levels and hypo-acetylation of non-histone proteins (or metabolites) may be important in solid tumors, whereas acetylation of histones is important in liquid tumors. We also note that the acetylation status and its effect on the function of non-histone proteins are largely unknown. Although approximately 13,000 and 11,000 acetylation sites have been identified, in mouse and human cell lines,[16,61,62] respectively, only about 100 acetylation sites have been functionally characterized.

We report that TEAD2 and E2A play an important role in HCC, in both patients and mouse models. We observed that changes in TEAD2 and E2A expression directly affect acetyl-CoA metabolism and thereby cell proliferation. *In vitro*, knockdown of

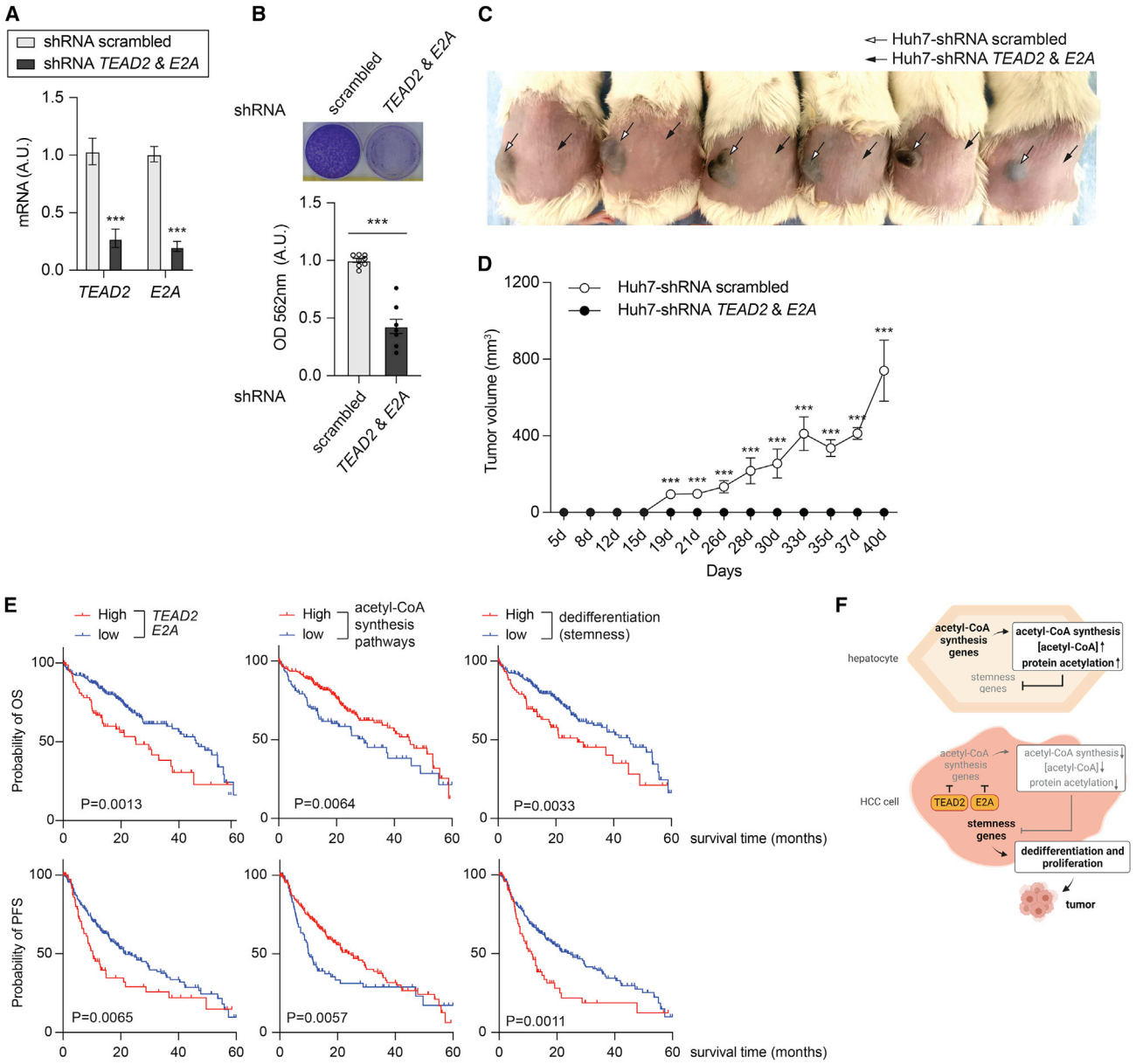

Figure 7. Knockdown of TEAD2 and E2A inhibites HCC cell xenograft growth in mice, and expressions of TEAD2 and E2A correlate with poor survival of HCC

(A) mRNA levels of *TEAD2* and *E2A* upon control (scrambled) and TEAD2&E2A double-knockdown in Huh7 cells. N = 5–6. Multiple t test, *** $p < 0.001$.

(B) Clonogenic growth assay upon control (scrambled) and TEAD2&E2A double-knockdown in Huh7 cells. N = 8. Student's t test, *** $p < 0.001$.

(C) Representative pictures of xenograft mice from subcutaneous injection of *TEAD2* and *E2A* double-knockdown (right flank, black arrow) and control (scrambled) expressing Huh7 cells (left flank, white arrow), n = 6.

(D) Tumor growth curves of subcutaneous xenografts derived from *TEAD2* and *E2A* double-knockdown (black circle) and control (scrambled) expressing Huh7 cells (white circle) in mice. The tumor volume was monitored at predetermined time points and was measured by caliper, n = 6 (three tumors were harvested at 33 days and rest three tumors were harvested at 40 days).

(E) Kaplan-Meier survival estimate curves for TCGA-LIHC patients ranked by expression of *TEAD2* and *E2A*, acetyl-CoA synthesis enzymes, and dedifferentiation (stemness) markers. Overall survival for *TEAD2* and *E2A*: n = 82 (high) and 243 (low), overall survival for average expression of acetyl-CoA synthesis enzymes: n = 215 (high) and 110 (low), and overall survival for average expression of dedifferentiation (stemness) markers: n = 84 (high) and 241 (low). p value according to the log-rank test. Progression free survival for *TEAD2* and *E2A*: n = 84 (high) and 263 (low), progression free survival for average expression of acetyl-CoA synthesis enzymes: n = 236 (high) and 111 (low), and progression free survival for average expression of dedifferentiation (stemness) markers: n = 85 (high) and 262 (low). p value according to the log-rank test.

(F) Illustration highlights metabolic differences along with protein acetylation and dedifferentiation in normal hepatocyte and HCC cells.

TEAD2 and *E2A* enhanced acetyl-CoA synthesis and reduced cell proliferation, whereas overexpression of TEAD2 and E2A suppressed acetyl-CoA synthesis and promoted cell proliferation (Figures 3, 4, and S3–S5). *In vivo*, knockdown of TEAD2 and E2A prevented tumor initiation and growth (Figures 7C and 7D). Thus, TEAD2 and E2A promote tumorigenesis via inhibition of acetyl-CoA synthesis and protein acetylation. TEAD2 and E2A were previously implicated in tumorigenesis, but via expression of EMT related genes.[63,64] The TEADs, of which there are four isozymes, are mediators of the Hippo pathway that regulate cell proliferation and organ size.[65] Among the TEADs, only TEAD2 was upregulated in HCC and negatively correlated with the overall survival of patients.[66] We report that TEAD2, but not other TEADs, suppresses acetyl-CoA synthesis and thereby reduces acetyl-CoA levels and protein acetylation (Figures 3A, 3B, 3E–3J, and S4A–S4I). Furthermore, suppression of acetyl-CoA synthesis genes by TEAD2 is independent of YAP/TAZ and VGLLs (Figures S4J–S4M).

The role of E2A in tumorigenesis has been controversial. E2A was first reported as a tumor suppressor in lymphoma.[67,68] However, it was later shown to be upregulated in prostate cancer[69] and cervical squamous cell carcinoma.[70] Furthermore, E2A promotes cell proliferation and tumor growth in LSCC but inhibits cell proliferation in lung adenocarcinoma,[71] suggesting that E2A impacts tumorigenesis in a cancer type-dependent manner. We observed that high TEAD2 and E2A expression negatively correlates with patient survival in HCC and LSCC, but not in B cell lymphoma and lung adenocarcinoma. In line with the observation that TEAD2 and E2A expression negatively correlates with patient survival, expression of acetyl-CoA synthesis genes positively correlates with patient survival (Figures 7E, S9C, and S9G). Our findings suggest that TEAD2 and E2A promote tumorigenesis via rewiring acetyl-CoA metabolism in several cancers. We note that neither TEAD2 nor E2A was previously implicated in acetyl-CoA synthesis.

Metabolic reprogramming is common and important in cancer cells. We demonstrate that metabolic changes in HCC are due to upregulation of TEAD2 and E2A, causing inhibition of acetyl-CoA synthesis and, in turn, dedifferentiation/stemness (Figure 7F). Previous reports suggest that the transcription factors TEAD2 and E2A maintain stem cell pools.[29,72,73] We note that expression of *TEAD2* and *E2A* is very low in hepatocytes compared with mouse embryos and human ES cells (Figures S9I and S9J).[74,75] We observed that TEAD2 and E2A induce expression of pluripotency transcription factors and cancer stem cell markers via lowering acetyl-CoA levels (Figures 5, 6, S7, and S8). Thus, our findings functionally link the dedifferentiated state of stem cells and cancer cells.

Limitations of the study

Our study identified transcriptional suppression of acetyl-CoA synthesis, reduction of acetyl-CoA levels, and hypo-acetylation of non-histone proteins in HCC. Follow-up studies are required to examine the function of hypo-acetylated proteins such as metabolic enzymes and pluripotency transcription factors. Furthermore, our study was conducted in HCC. Whether the same transcriptional suppression of acetyl-CoA synthesis can be generalized to other cancers remains to be addressed, although TCGA mRNA expression and patient survival data suggest that it is common (Figures S9A–S9D). Shedding light on these questions might uncover therapeutic options in targeting TEAD2 and E2A and/or acetyl-CoA metabolism.

STAR★METHODS

Detailed methods are provided in the online version of this paper and include the following:

- KEY RESOURCES TABLE
- RESOURCE AVAILABILITY
  - Lead contact
  - Materials availability
  - Data and code availability
- EXPERIMENTAL MODEL AND SUBJECT DETAILS
  - Animals
  - Human and mouse HCC cell lines
  - Patient material and ethics
- METHOD DETAILS
  - Immunoblot analysis
  - H&E staining and immunohistochemistry (IHC)
  - Fluorescence activated cell sorting (FACS)
  - HCC xenografts in NOD/SCID gamma-c (NSG) mice
  - Immunoprecipitation (IP)
  - Stable TEAD2 or E2A overexpression or knockdown cells
  - Stable *PDK1* and *PDK2* knockdown cells
  - Transient ACSS2 overexpression cells
  - Transient transfection and luciferase reporter constructs
  - Cell treatments
  - Clonogenic growth assay and crystal violet staining
  - RNA isolation and quantitative reverse transcriptase PCR
  - Metabolites and enzyme activity assays
  - Mouse proteome and transcriptome
  - Mouse acetylome
  - Metabolomics of mouse liver tissues
  - Proteome of patient tumor tissue
  - RNA-sequencing and data processing of patient samples
  - Patient survival analyses
  - Correlation with *TEAD2* or *E2A* and binding site prediction
- QUANTIFICATION AND STATISTICAL ANALYSIS

SUPPLEMENTAL INFORMATION

Supplemental information can be found online at https://doi.org/10.1016/j.molcel.2022.10.027.

ACKNOWLEDGMENTS

S.P. acknowledges support from the University of Basel Forschungsfonds. D.M. acknowledges support from the German Research Foundation (DFG). M.N.H. acknowledges the European Research Council (MERiC), the Swiss National Science Foundation, SystemsX.ch, and the Louis-Jeantet Foundation. We are grateful to Fengyuan Tang and Gerhard Christofori for providing important reagents.

AUTHOR CONTRIBUTIONS

S.P. and M.N.H. conceived and designed the experiments. S.P., D.M., and M.N.H. wrote the manuscript. S.P., Q.C., X.W., E.D., D.M., M.C., B.R., C.K.Y.N., and A.S. performed experiments and analyzed data. L.M.T. and M.H.H. provided reagents and human HCC patient samples. All authors approved the manuscript.

DECLARATION OF INTERESTS

The authors declare no competing interests.

Received: March 30, 2022
Revised: August 22, 2022
Accepted: October 24, 2022
Published: November 17, 2022

REFERENCES

1. Sivanand, S., Viney, I., and Wellen, K.E. (2018). Spatiotemporal control of acetyl-CoA metabolism in chromatin regulation. Trends Biochem. Sci. *43*, 61–74. https://doi.org/10.1016/j.tibs.2017.11.004.
2. Ericksen, R.E., Lim, S.L., McDonnell, E., Shuen, W.H., Vadiveloo, M., White, P.J., Ding, Z., Kwok, R., Lee, P., Radda, G.K., et al. (2019). Loss of BCAA catabolism during carcinogenesis enhances mTORC1 activity and promotes tumor development and progression. Cell Metab. *29*, 1151–1165.e6. https://doi.org/10.1016/j.cmet.2018.12.020.
3. Li, J.T., Yin, M., Wang, D., Wang, J., Lei, M.Z., Zhang, Y., Liu, Y., Zhang, L., Zou, S.W., Hu, L.P., et al. (2020). BCAT2-mediated BCAA catabolism is critical for development of pancreatic ductal adenocarcinoma. Nat. Cell Biol. *22*, 167–174. https://doi.org/10.1038/s41556-019-0455-6.
4. Aiderus, A., Black, M.A., and Dunbier, A.K. (2018). Fatty acid oxidation is associated with proliferation and prognosis in breast and other cancers. BMC Cancer *18*, 805. https://doi.org/10.1186/s12885-018-4626-9.
5. Fujiwara, N., Nakagawa, H., Enooku, K., Kudo, Y., Hayata, Y., Nakatsuka, T., Tanaka, Y., Tateishi, R., Hikiba, Y., Misumi, K., et al. (2018). CPT2 downregulation adapts HCC to lipid-rich environment and promotes carcinogenesis via acylcarnitine accumulation in obesity. Gut *67*, 1493–1504. https://doi.org/10.1136/gutjnl-2017-315193.
6. Park, J.H., Vithayathil, S., Kumar, S., Sung, P.L., Dobrolecki, L.E., Putluri, V., Bhat, V.B., Bhowmik, S.K., Gupta, V., Arora, K., et al. (2016). Fatty acid oxidation-driven Src links mitochondrial energy reprogramming and oncogenic properties in triple-negative breast cancer. Cell Rep. *14*, 2154–2165. https://doi.org/10.1016/j.celrep.2016.02.004.
7. Shao, H., Mohamed, E.M., Xu, G.G., Waters, M., Jing, K., Ma, Y., Zhang, Y., Spiegel, S., Idowu, M.O., and Fang, X. (2016). Carnitine palmitoyltransferase 1A functions to repress FoxO transcription factors to allow cell cycle progression in ovarian cancer. Oncotarget *7*, 3832–3846. https://doi.org/10.18632/oncotarget.6757.
8. Woolbright, B.L., Rajendran, G., Harris, R.A., and Taylor, J.A., 3rd (2019). Metabolic flexibility in cancer: targeting the pyruvate dehydrogenase kinase:pyruvate dehydrogenase axis. Mol. Cancer Ther. *18*, 1673–1681. https://doi.org/10.1158/1535-7163.MCT-19-0079.
9. Huch, M., Gehart, H., van Boxtel, R., Hamer, K., Blokzijl, F., Verstegen, M.M., Ellis, E., van Wenum, M., Fuchs, S.A., de Ligt, J., et al. (2015). Long-term culture of genome-stable bipotent stem cells from adult human liver. Cell *160*, 299–312. https://doi.org/10.1016/j.cell.2014.11.050.
10. Liu, M., Yan, Q., Sun, Y., Nam, Y., Hu, L., Loong, J.H., Ouyang, Q., Zhang, Y., Li, H.L., Kong, F.E., et al. (2020). A hepatocyte differentiation model reveals two subtypes of liver cancer with different oncofetal properties and therapeutic targets. Proc. Natl. Acad. Sci. USA *117*, 6103–6113. https://doi.org/10.1073/pnas.1912146117.
11. Yamashita, T., Ji, J., Budhu, A., Forgues, M., Yang, W., Wang, H.Y., Jia, H., Ye, Q., Qin, L.X., Wauthier, E., et al. (2009). EpCAM-positive hepatocellular carcinoma cells are tumor-initiating cells with stem/progenitor cell features. Gastroenterology *136*, 1012–1024. https://doi.org/10.1053/j.gastro.2008.12.004.
12. Dimitrakopoulos, C., Hindupur, S.K., Colombi, M., Liko, D., Ng, C.K.Y., Piscuoglio, S., Behr, J., Moore, A.L., Singer, J., Ruscheweyh, H.J., et al. (2021). Multi-omics data integration reveals novel drug targets in hepatocellular carcinoma. BMC Genomics *22*, 592. https://doi.org/10.1186/s12864-021-07876-9.
13. Guri, Y., Colombi, M., Dazert, E., Hindupur, S.K., Roszik, J., Moes, S., Jenoe, P., Heim, M.H., Riezman, I., Riezman, H., et al. (2017). mTORC2 promotes tumorigenesis via lipid synthesis. Cancer Cell *32*, 807–823.e12. https://doi.org/10.1016/j.ccell.2017.11.011.
14. Hindupur, S.K., Colombi, M., Fuhs, S.R., Matter, M.S., Guri, Y., Adam, K., Cornu, M., Piscuoglio, S., Ng, C.K.Y., Betz, C., et al. (2018). The protein histidine phosphatase LHPP is a tumour suppressor. Nature *555*, 678–682. https://doi.org/10.1038/nature26140.
15. Christensen, D.G., Xie, X., Basisty, N., Byrnes, J., McSweeney, S., Schilling, B., and Wolfe, A.J. (2019). Post-translational protein acetylation: an elegant mechanism for bacteria to dynamically regulate metabolic functions. Front. Microbiol. *10*, 1604. https://doi.org/10.3389/fmicb.2019.01604.
16. Narita, T., Weinert, B.T., and Choudhary, C. (2019). Functions and mechanisms of non-histone protein acetylation. Nat. Rev. Mol. Cell Biol. *20*, 156–174. https://doi.org/10.1038/s41580-018-0081-3.
17. Shvedunova, M., and Akhtar, A. (2022). Modulation of cellular processes by histone and non-histone protein acetylation. Nat. Rev. Mol. Cell Biol. *23*, 329–349. https://doi.org/10.1038/s41580-021-00441-y.
18. Bulusu, V., Tumanov, S., Michalopoulou, E., van den Broek, N.J., MacKay, G., Nixon, C., Dhayade, S., Schug, Z.T., Vande Voorde, J., Blyth, K., et al. (2017). Acetate recapturing by nuclear acetyl-CoA synthetase 2 prevents loss of histone acetylation during oxygen and serum limitation. Cell Rep. *18*, 647–658. https://doi.org/10.1016/j.celrep.2016.12.055.
19. Ng, C.K.Y., Dazert, E., Boldanova, T., Coto-Llerena, M., Nuciforo, S., Ercan, C., Suslov, A., Meier, M.A., Bock, T., Schmidt, A., et al. (2022). Integrative proteogenomic characterization of hepatocellular carcinoma across etiologies and stages. Nat. Commun. *13*, 2436. https://doi.org/10.1038/s41467-022-29960-8.
20. Sivanand, S., and Vander Heiden, M.G. (2020). Emerging roles for branched-chain amino acid metabolism in cancer. Cancer Cell *37*, 147–156. https://doi.org/10.1016/j.ccell.2019.12.011.
21. Pietrocola, F., Galluzzi, L., Bravo-San Pedro, J.M., Madeo, F., and Kroemer, G. (2015). Acetyl coenzyme A: a central metabolite and second messenger. Cell Metab. *21*, 805–821. https://doi.org/10.1016/j.cmet.2015.05.014.
22. Klyuyeva, A., Tuganova, A., Kedishvili, N., and Popov, K.M. (2019). Tissue-specific kinase expression and activity regulate flux through the pyruvate dehydrogenase complex. J. Biol. Chem. *294*, 838–851. https://doi.org/10.1074/jbc.RA118.006433.
23. Sutendra, G., and Michelakis, E.D. (2013). Pyruvate dehydrogenase kinase as a novel therapeutic target in oncology. Front. Oncol. *3*, 38. https://doi.org/10.3389/fonc.2013.00038.
24. Seifert, F., Ciszak, E., Korotchkina, L., Golbik, R., Spinka, M., Dominiak, P., Sidhu, S., Brauer, J., Patel, M.S., and Tittmann, K. (2007). Phosphorylation of serine 264 impedes active site accessibility in the E1 component of the human pyruvate dehydrogenase multienzyme complex. Biochemistry *46*, 6277–6287. https://doi.org/10.1021/bi700083z.
25. Kolb, H., Kempf, K., Röhling, M., Lenzen-Schulte, M., Schloot, N.C., and Martin, S. (2021). Ketone bodies: from enemy to friend and guardian angel. BMC Med. *19*, 313. https://doi.org/10.1186/s12916-021-02185-0.
26. Bosron, W.F., and Li, T.K. (1986). Genetic polymorphism of human liver alcohol and aldehyde dehydrogenases, and their relationship to alcohol metabolism and alcoholism. Hepatology *6*, 502–510. https://doi.org/10.1002/hep.1840060330.

27. Luong, A., Hannah, V.C., Brown, M.S., and Goldstein, J.L. (2000). Molecular characterization of human acetyl-CoA synthetase, an enzyme regulated by sterol regulatory element-binding proteins. J. Biol. Chem. *275*, 26458–26466. https://doi.org/10.1074/jbc.M004160200.

28. Moffett, J.R., Puthillathu, N., Vengilote, R., Jaworski, D.M., and Namboodiri, A.M. (2020). Acetate revisited: A key biomolecule at the nexus of metabolism, epigenetics and oncogenesis-part 1: acetyl-CoA, acetogenesis and acyl-CoA short-chain synthetases. Front. Physiol. *11*, 580167. https://doi.org/10.3389/fphys.2020.580167.

29. Alder, O., Cullum, R., Lee, S., Kan, A.C., Wei, W., Yi, Y., Garside, V.C., Bilenky, M., Griffith, M., Morrissy, A.S., et al. (2014). Hippo signaling influences HNF4A and FOXA2 enhancer switching during hepatocyte differentiation. Cell Rep. *9*, 261–271. https://doi.org/10.1016/j.celrep.2014.08.046.

30. Sun, L., Kong, Y., Cao, M., Zhou, H., Li, H., Cui, Y., Fang, F., Zhang, W., Li, J., Zhu, X., et al. (2017). Decreased expression of acetyl-CoA synthase 2 promotes metastasis and predicts poor prognosis in hepatocellular carcinoma. Cancer Sci. *108*, 1338–1346. https://doi.org/10.1111/cas.13252.

31. Comerford, S.A., Huang, Z., Du, X., Wang, Y., Cai, L., Witkiewicz, A.K., Walters, H., Tantawy, M.N., Fu, A., Manning, H.C., et al. (2014). Acetate dependence of tumors. Cell *159*, 1591–1602. https://doi.org/10.1016/j.cell.2014.11.020.

32. Gao, X., Lin, S.H., Ren, F., Li, J.T., Chen, J.J., Yao, C.B., Yang, H.B., Jiang, S.X., Yan, G.Q., Wang, D., et al. (2016). Acetate functions as an epigenetic metabolite to promote lipid synthesis under hypoxia. Nat. Commun. *7*, 11960. https://doi.org/10.1038/ncomms11960.

33. Wang, Y.H., Huang, S., Zhu, L., Yang, Q., Yang, X.M., Gu, J.R., Zhang, Z.G., Nie, H.Z., and Li, J. (2019). Alternative transcription start site selection in ACSS2 controls its nuclear localization and promotes ribosome biosynthesis in hepatocellular carcinoma. Biochem. Biophys. Res. Commun. *514*, 632–638. https://doi.org/10.1016/j.bbrc.2019.04.193.

34. Barrero, M.J., Camarero, N., Marrero, P.F., and Haro, D. (2003). Control of human carnitine palmitoyltransferase II gene transcription by peroxisome proliferator-activated receptor through a partially conserved peroxisome proliferator-responsive element. Biochem. J. *369*, 721–729. https://doi.org/10.1042/BJ20020851.

35. Kim, M., Kim, T., Johnson, R.L., and Lim, D.S. (2015). Transcriptional co-repressor function of the hippo pathway transducers YAP and TAZ. Cell Rep. *11*, 270–282. https://doi.org/10.1016/j.celrep.2015.03.015.

36. Rao, C., Malaguti, M., Mason, J.O., and Lowell, S. (2020). The transcription factor E2A drives neural differentiation in pluripotent cells. Development *147*. https://doi.org/10.1242/dev.184093.

37. Wills, A.E., and Baker, J.C. (2015). E2a is necessary for Smad2/3-dependent transcription and the direct repression of lefty during gastrulation. Dev. Cell *32*, 345–357. https://doi.org/10.1016/j.devcel.2014.11.034.

38. Zanconato, F., Cordenonsi, M., and Piccolo, S. (2019). YAP and TAZ: a signalling hub of the tumour microenvironment. Nat. Rev. Cancer *19*, 454–464. https://doi.org/10.1038/s41568-019-0168-y.

39. Yong, K.J., Gao, C., Lim, J.S., Yan, B., Yang, H., Dimitrov, T., Kawasaki, A., Ong, C.W., Wong, K.F., Lee, S., et al. (2013). Oncofetal gene SALL4 in aggressive hepatocellular carcinoma. N. Engl. J. Med. *368*, 2266–2276. https://doi.org/10.1056/NEJMoa1300297.

40. Asai, R., Tsuchiya, H., Amisaki, M., Makimoto, K., Takenaga, A., Sakabe, T., Hoi, S., Koyama, S., and Shiota, G. (2019). CD44 standard isoform is involved in maintenance of cancer stem cells of a hepatocellular carcinoma cell line. Cancer Med. *8*, 773–782. https://doi.org/10.1002/cam4.1968.

41. Haramaki, M., Yano, H., Fukuda, K., Momosaki, S., Ogasawara, S., and Kojiro, M. (1995). Expression of CD44 in human hepatocellular-carcinoma cell-lines. Hepatology *21*, 1276–1284.

42. Yan, Y., Li, Z., Kong, X., Jia, Z., Zuo, X., Gagea, M., Huang, S., Wei, D., and Xie, K. (2016). KLF4-mediated suppression of CD44 signaling negatively impacts pancreatic cancer stemness and metastasis. Cancer Res. *76*, 2419–2431. https://doi.org/10.1158/0008-5472.CAN-15-1691.

43. Zhao, S., Chen, C., Chang, K., Karnad, A., Jagirdar, J., Kumar, A.P., and Freeman, J.W. (2016). CD44 expression level and isoform contributes to pancreatic cancer cell plasticity, invasiveness, and response to therapy. Clin. Cancer Res. *22*, 5592–5604. https://doi.org/10.1158/1078-0432.CCR-15-3115.

44. Baltus, G.A., Kowalski, M.P., Zhai, H., Tutter, A.V., Quinn, D., Wall, D., and Kadam, S. (2009). Acetylation of sox2 induces its nuclear export in embryonic stem cells. Stem Cells *27*, 2175–2184. https://doi.org/10.1002/stem.168.

45. Williams, E.G., Wu, Y., Jha, P., Dubuis, S., Blattmann, P., Argmann, C.A., Houten, S.M., Amariuta, T., Wolski, W., Zamboni, N., et al. (2016a). Systems proteomics of liver mitochondria function. Science *352*, aad0189. https://doi.org/10.1126/science.aad0189.

46. Williams, E.O., Taylor, A.K., Bell, E.L., Lim, R., Kim, D.M., and Guarente, L. (2016b). Sirtuin 1 promotes deacetylation of Oct4 and maintenance of naive pluripotency. Cell Rep. *17*, 809–820. https://doi.org/10.1016/j.celrep.2016.09.046.

47. Zhao, S., Xu, W., Jiang, W., Yu, W., Lin, Y., Zhang, T., Yao, J., Zhou, L., Zeng, Y., Li, H., et al. (2010). Regulation of cellular metabolism by protein lysine acetylation. Science *327*, 1000–1004. https://doi.org/10.1126/science.1179689.

48. Cimen, H., Han, M.J., Yang, Y., Tong, Q., Koc, H., and Koc, E.C. (2010). Regulation of succinate dehydrogenase activity by SIRT3 in mammalian mitochondria. Biochemistry *49*, 304–311. https://doi.org/10.1021/bi901627u.

49. Kerr, M., Miller, J.J., Thapa, D., Stiewe, S., Timm, K.N., Aparicio, C.N.M., Scott, I., Tyler, D.J., and Heather, L.C. (2020). Rescue of myocardial energetic dysfunction in diabetes through the correction of mitochondrial hyperacetylation by honokiol. JCI Insight *5*. e140326. https://doi.org/10.1172/jci.insight.140326.

50. Vassilopoulos, A., Pennington, J.D., Andresson, T., Rees, D.M., Bosley, A.D., Fearnley, I.M., Ham, A., Flynn, C.R., Hill, S., Rose, K.L., et al. (2014). SIRT3 deacetylates ATP synthase F1 complex proteins in response to nutrient- and exercise-induced stress. Antioxid. Redox Signal. *21*, 551–564. https://doi.org/10.1089/ars.2013.5420.

51. Zhang, X., Jiang, L., Huang, K., Fang, C., Li, J., Yang, J., Li, H., Ruan, X., Wang, P., Mo, M., et al. (2020). Site-selective phosphoglycerate mutase 1 acetylation by a small molecule. ACS Chem. Biol. *15*, 632–639. https://doi.org/10.1021/acschembio.9b00962.

52. Berthiaume, J.M., Hsiung, C.H., Austin, A.B., McBrayer, S.P., Depuydt, M.M., Chandler, M.P., Miyagi, M., and Rosca, M.G. (2017). Methylene blue decreases mitochondrial lysine acetylation in the diabetic heart. Mol. Cell. Biochem. *432*, 7–24. https://doi.org/10.1007/s11010-017-2993-1.

53. Fu, Z., Runquist, J.A., Montgomery, C., Miziorko, H.M., and Kim, J.J. (2010). Functional insights into human HMG-CoA lyase from structures of acyl-CoA-containing ternary complexes. J. Biol. Chem. *285*, 26341–26349. https://doi.org/10.1074/jbc.M110.139931.

54. Cui, Y., Qin, L., Wu, J., Qu, X., Hou, C., Sun, W., Li, S., Vaughan, A.T., Li, J.J., and Liu, J. (2015). SIRT3 enhances glycolysis and proliferation in SIRT3-expressing gastric cancer cells. PLoS One *10*, e0129834. https://doi.org/10.1371/journal.pone.0129834.

55. Parodi-Rullán, R.M., Chapa-Dubocq, X.R., and Javadov, S. (2018). Acetylation of mitochondrial proteins in the heart: the role of SIRT3. Front. Physiol. *9*, 1094. https://doi.org/10.3389/fphys.2018.01094.

56. Ren, X., Wang, X., Peng, B., Liang, Q., Cai, Y., Gao, K., Hu, Y., Xu, Z., and Yan, Y. (2021). Significance of TEAD family in diagnosis, prognosis and immune response for ovarian serous carcinoma. Int. J. Gen. Med. *14*, 7133–7143. https://doi.org/10.2147/IJGM.S336602.

57. Sheikh, B.N., and Akhtar, A. (2019). The many lives of KATs - detectors, integrators and modulators of the cellular environment. Nat. Rev. Genet. *20*, 7–23. https://doi.org/10.1038/s41576-018-0072-4.

58. Tsilimigras, D.I., Ntanasis-Stathopoulos, I., Moris, D., Spartalis, E., and Pawlik, T.M. (2018). Histone deacetylase inhibitors in hepatocellular carcinoma: a therapeutic perspective. Surg. Oncol. *27*, 611–618. https://doi.org/10.1016/j.suronc.2018.07.015.

59. West, A.C., and Johnstone, R.W. (2014). New and emerging HDAC inhibitors for cancer treatment. J. Clin. Invest. *124*, 30–39. https://doi.org/10.1172/JCI69738.

60. Suraweera, A., O'Byrne, K.J., and Richard, D.J. (2018). Combination therapy With histone deacetylase inhibitors (HDACi) for the treatment of cancer: achieving the full therapeutic potential of HDACi. Front. Oncol. *8*, 92. https://doi.org/10.3389/fonc.2018.00092.

61. Ali, I., Conrad, R.J., Verdin, E., and Ott, M. (2018). Lysine acetylation goes global: From epigenetics to metabolism and therapeutics. Chem. Rev. *118*, 1216–1252. https://doi.org/10.1021/acs.chemrev.7b00181.

62. Baeza, J., Smallegan, M.J., and Denu, J.M. (2016). Mechanisms and dynamics of protein acetylation in mitochondria. Trends Biochem. Sci. *41*, 231–244. https://doi.org/10.1016/j.tibs.2015.12.006.

63. Diepenbruck, M., Waldmeier, L., Ivanek, R., Berninger, P., Arnold, P., van Nimwegen, E., and Christofori, G. (2014). Tead2 expression levels control the subcellular distribution of Yap and Taz, zyxin expression and epithelial-mesenchymal transition. J. Cell Sci. *127*, 1523–1536. https://doi.org/10.1242/jcs.139865.

64. Perez-Moreno, M.A., Locascio, A., Rodrigo, I., Dhondt, G., Portillo, F., Nieto, M.A., and Cano, A. (2001). A new role for E12/E47 in the repression of E-cadherin expression and epithelial-mesenchymal transitions. J. Biol. Chem. *276*, 27424–27431. https://doi.org/10.1074/jbc.M100827200.

65. Ma, S., Meng, Z., Chen, R., and Guan, K.L. (2019). The hippo pathway: biology and pathophysiology. Annu. Rev. Biochem. *88*, 577–604. https://doi.org/10.1146/annurev-biochem-013118-111829.

66. Joo, J.S., Cho, S.Y., Rou, W.S., Kim, J.S., Kang, S.H., Lee, E.S., Moon, H.S., Kim, S.H., Sung, J.K., Kwon, I.S., et al. (2020). TEAD2 as a novel prognostic factor for hepatocellular carcinoma. Oncol. Rep. *43*, 1785–1796. https://doi.org/10.3892/or.2020.7578.

67. Bain, G., Maandag, E.C., Izon, D.J., Amsen, D., Kruisbeek, A.M., Weintraub, B.C., Krop, I., Schlissel, M.S., Feeney, A.J., van Roon, M., et al. (1994). E2A proteins are required for proper B cell development and initiation of immunoglobulin gene rearrangements. Cell *79*, 885–892. https://doi.org/10.1016/0092-8674(94)90077-9.

68. Engel, I., and Murre, C. (1999). Ectopic expression of E47 or E12 promotes the death of E2A-deficient lymphomas. Proc. Natl. Acad. Sci. USA *96*, 996–1001. https://doi.org/10.1073/pnas.96.3.996.

69. Patel, D., and Chaudhary, J. (2012). Increased expression of bHLH transcription factor E2A (TCF3) in prostate cancer promotes proliferation and confers resistance to doxorubicin induced apoptosis. Biochem. Biophys. Res. Commun. *422*, 146–151. https://doi.org/10.1016/j.bbrc.2012.04.126.

70. Luo, L., Zhang, H., Nian, S., Lv, C., Ni, B., Wang, D., and Tian, Z. (2017). Up-regulation of transcription factor 3 is correlated With poor prognosis in cervical carcinoma. Int. J. Gynecol. Cancer *27*, 1422–1430. https://doi.org/10.1097/IGC.0000000000001032.

71. Xu, J., Li, F., Gao, Y., Guo, R., Ding, L., Fu, M., Yi, Y., Chen, H., Xiao, Z.J., and Niu, M. (2021). E47 upregulates DeltaNp63alpha to promote growth of squamous cell carcinoma. Cell Death Dis. *12*, 381. https://doi.org/10.1038/s41419-021-03662-3.

72. Semerad, C.L., Mercer, E.M., Inlay, M.A., Weissman, I.L., and Murre, C. (2009). E2A proteins maintain the hematopoietic stem cell pool and promote the maturation of myelolymphoid and myeloerythroid progenitors. Proc. Natl. Acad. Sci. USA *106*, 1930–1935. https://doi.org/10.1073/pnas.0808866106.

73. Tamm, C., Böwer, N., and Annerén, C. (2011). Regulation of mouse embryonic stem cell self-renewal by a Yes-YAP-TEAD2 signaling pathway downstream of LIF. J. Cell Sci. *124*, 1136–1144. https://doi.org/10.1242/jcs.075796.

74. Godoy, P., Schmidt-Heck, W., Natarajan, K., Lucendo-Villarin, B., Szkolnicka, D., Asplund, A., Björquist, P., Widera, A., Stöber, R., Campos, G., et al. (2015). Gene networks and transcription factor motifs defining the differentiation of stem cells into hepatocyte-like cells. J. Hepatol. *63*, 934–942. https://doi.org/10.1016/j.jhep.2015.05.013.

75. Yue, F., Cheng, Y., Breschi, A., Vierstra, J., Wu, W., Ryba, T., Sandstrom, R., Ma, Z., Davis, C., Pope, B.D., et al. (2014). A comparative encyclopedia of DNA elements in the mouse genome. Nature *515*, 355–364. https://doi.org/10.1038/nature13992.

76. Nuciforo, S., Fofana, I., Matter, M.S., Blumer, T., Calabrese, D., Boldanova, T., Piscuoglio, S., Wieland, S., Ringnalda, F., Schwank, G., et al. (2018). Organoid models of human liver cancers derived from tumor needle biopsies. Cell Rep. *24*, 1363–1376. https://doi.org/10.1016/j.celrep.2018.07.001.

77. European Association for the Study of the Liver (2018). EASL clinical practice guidelines: management of hepatocellular carcinoma. J. Hepatol. *69*, 182–236. https://doi.org/10.1016/j.jhep.2018.03.019.

78. Ahrné, E., Glatter, T., Viganò, C., Schubert, Cv, Nigg, E.A., and Schmidt, A. (2016). Evaluation and improvement of quantification accuracy in isobaric mass tag-based protein quantification experiments. J. Proteome Res. *15*, 2537–2547. https://doi.org/10.1021/acs.jproteome.6b00066.

79. Fuhrer, T., Heer, D., Begemann, B., and Zamboni, N. (2011). High-throughput, accurate mass metabolome profiling of cellular extracts by flow injection-time-of-flight mass spectrometry. Anal. Chem. *83*, 7074–7080. https://doi.org/10.1021/ac201267k.

80. Dazert, E., Colombi, M., Boldanova, T., Moes, S., Adametz, D., Quagliata, L., Roth, V., Terracciano, L., Heim, M.H., Jenoe, P., and Hall, M.N. (2016). Quantitative proteomics and phosphoproteomics on serial tumor biopsies from a sorafenib-treated HCC patient. Proc. Natl. Acad. Sci. USA *113*, 1381–1386. https://doi.org/10.1073/pnas.1523434113.

81. Gillet, L.C., Navarro, P., Tate, S., Röst, H., Selevsek, N., Reiter, L., Bonner, R., and Aebersold, R. (2012). Targeted data extraction of the MS/MS spectra generated by data-independent acquisition: a new concept for consistent and accurate proteome analysis. Mol. Cell. Proteomics *11*. O111.016717. https://doi.org/10.1074/mcp.O111.016717.

STAR★METHODS

KEY RESOURCES TABLE

REAGENT or RESOURCE	SOURCE	IDENTIFIER
Antibodies		
Rabbit anti-acetylated lysine	Cell Signaling Technology	Cat# 9441; RRID:AB_331805
Rabbit anti-ACSL1	Cell Signaling Technology	Cat# 9189; RRID:AB_10891616
Rabbit anti-ACSS2	Cell Signaling Technology	Cat# 3658; RRID:AB_2222710
Rabbit anti-Albumin	Cell Signaling Technology	Cat# 4929; RRID:AB_2225785
Rabbit anti-CD44	Cell Signaling Technology	Cat# 37259; RRID:AB_2750879
Alexa 555 conjugated anti-CD44 antibody	Cell Signaling Technology	Cat# 95235
Rabbit anti-Histone H3	Cell Signaling Technology	Cat# 4499; RRID:AB_10544537
Rabbit anti-Histone H4	Cell Signaling Technology	Cat# 2592; RRID:AB_2118614
Rabbit anti-Pan TEAD	Cell Signaling Technology	Cat# 13295; RRID:AB_2687902
Rabbit anti-SALL4	Cell Signaling Technology	Cat# 5850; RRID:AB_10858883
Rabbit anti-SLUG	Cell Signaling Technology	Cat# 9585; RRID:AB_2239535
Rabbit anti-pYAP S127	Cell Signaling Technology	Cat# 4911; RRID:AB_2218913
Rabbit anti-YAP	Cell Signaling Technology	Cat# 4912; RRID:AB_2218911
Rabbit anti-ACAA2	Abcam	Cat# ab128911; RRID:AB_11143433
Rabbit anti-ACADSB	Abcam	Cat# ab99951; RRID:AB_10676013
Rabbit anti-acetylated lysine	Abcam	# ab21623, ab190479; RRID:AB_446436
Rabbit anti-EpCAM	Abcam	Cat# ab71916; RRID:AB_1603782
Rabbit anti-N-cadherin	Abcam	Cat# ab76011; RRID:AB_1310479
Rabbit anti-OCT4	Abcam	Cat3 ab181557; RRID:AB_2687916
Rabbit anti-pPDHA1 S293	Abcam	Cat# ab177461; RRID:AB_2756339
Rabbit anti-PDHA1	Abcam	Cat# ab168379
Rabbit anti-E2A	Abcam	Cat# ab69999; RRID:AB_1271195
Rabbit anti-ACADVL	Genetex	Cat# GTX114232; RRID:AB_10620453
Rabbit anti-AUH	Genetex	Cat# GTX55527
Rabbit anti-IVD	Genetex	Cat# GTX114502; RRID:AB_10619570
Rabbit anti-HMGCL	Genetex	Cat# GTX109096; RRID:AB_1950501
Mouse anti-ACAD8	Santacruz Biotechnology	Cat# sc390038
Mouse anti-ALDH2	Santacruz Biotechnology	Cat# sc100496; RRID:AB_2242451
Mouse anti-CPT1	Santacruz Biotechnology	Cat# sc393070
Mouse anti-CPT2	Santacruz Biotechnology	Cat# sc377294
Mouse anti-CYP1A2	Santacruz Biotechnology	Cat# sc53241; RRID:AB_629359
Mouse anti-CYP3A4	Santacruz Biotechnology	Cat# sc53850; RRID:AB_782375
Mouse anti-HCD2 (ERAB)	Santacruz Biotechnology	Cat# sc136326; RRID:AB_10647087
Mouse anti-HIBADH	Santacruz Biotechnology	Cat# sc398288
Mouse anti-HIBCH	Santacruz Biotechnology	Cat# sc515355
Mouse anti-MCCC1	Santacruz Biotechnology	Cat# sc365754; RRID:AB_10841913
Mouse anti-MCCC2	Santacruz Biotechnology	Cat# sc390836
Mouse anti-NANOG	Santacruz Biotechnology	Cat# sc53850; RRID:AB_782375
Rabbit anti-OCT3/4	Santacruz Biotechnology	Cat# sc5279; RRID:AB_628051
Mouse anti-PDK1	Santacruz Biotechnology	Cat# sc515944
Mouse anti-PDK2	Santacruz Biotechnology	Cat# sc517284
Mouse anti-PPARa	Santacruz Biotechnology	Cat# sc398394;RRID:AB_2885073
Rabbit anti-acetyl-Histone H3	Sigma-Aldrich	Cat# 06-599

(*Continued on next page*)

Continued

REAGENT or RESOURCE	SOURCE	IDENTIFIER
Rabbit anti-acetyl-Histone H4	Sigma-Aldrich	Cat# 06-866
Rabbit anti-ACAT1	Sigma-Aldrich	Cat# HPA004428; RRID:AB_1078088
Rabbit anti-SOX2	Sigma-Aldrich	Cat# HPA045725
Rabbit anti-E2A	Sigma-Aldrich	Cat# HPA30014
Rabbit anti-BDH1	Thermo Fisher	Cat# MA5-15594; RRID:AB_11007633
Rabbit anti-ECHS1	Thermo Fisher	PA5-30014
Rabbit anti-TEAD2	Thermo Fisher	PA5-116018; RRID:AB_2900652
Mouse anti-Actin	Millipore	Cat# MAB1501; RRID:AB_2223041
Rabbit anti-SOX9	Millipore	Cat# AB5535; RRID:AB_2239761
Rabbit anti-Calnexin	Enzo	Cat# ADI-SPA-860; RRID:AB_10616095
Rabbit anti-VGLL4	ATLAS antibodies	Cat# HPA038614; RRID:AB_2676115
Goat anti mouse IgG HRP	Jackson immunoresearch	Cat# 115-035-174; RRID:AB_2338512
Goat anti rabbit IgG HRP	Jackson immunoresearch	Cat# 211-032-171; RRID:AB_2339149
Rabbit anti-TEAD2	Prof. Gerhard Christophori (University of Basel, Switzerland)	N/A
Bacterial and virus strains		
TCF3 (E2A) - Human, 4 unique 29mer shRNA constructs in lentiviral GFP vector	Origene	TL308904
TEAD2 - Human, 4 unique 29mer shRNA constructs in lentiviral GFP vector	Origene	TL308887
SMARTpool: ON-TARGETplus TCF3 siRNA	Horizon	L-009384-00-0005 5 nmol
SMARTpool: ON-TARGETplus TEAD2 siRNA	Horizon	L-012611-01-0005 5 nmol
Tead2 - Mouse, 4 unique 29mer shRNA constructs in retroviral untagged vector	Origene	TR502250
Tcf3 - Mouse, 4 unique 29mer shRNA constructs in retroviral untagged vector	Origene	TL510854
ORF expression clone for TCF3(NM_001136139.2) (Lenti viral, CMV, Purified plasmid)	GeneCopoeia	EX-Y4553-Lv197
ORF expression clone for TEAD2(NM_001256658.1) (Lenti viral, CMV, Purified plasmid)	GeneCopoeia	EX-Y5108-Lv126
ORF expression clone for mouse TCF3(NM_001164147.1) (Lenti viral, CMV, Purified plasmid)	GeneCopoeia	EX-Mm29752-Lv126
ORF expression clone for mouse TEAD2(NM_011565.2) (Lenti viral, CMV, Purified plasmid)	GeneCopoeia	EX-Mm05656-Lv126
MERCK mission shRNA bacterial stock for human PPARa	Sigma-Aldrich	TRCN0000001665, TRCN0000001667, TRCN0000001668, TRCN0000244945
MISSION® pLKO.1-puro Non-Target shRNA Control Plasmid DNA	Sigma-Aldrich	SHC016
ON-TARGETplus Non-targeting Control Pool	Horizon	D-001810-10-05
Non-effective 29-mer Scrambled shRNA Cassette in p-RFP-C-shLenti Vector, 5 ug	Origene	TR30031
Control vector (with EGFP) for pReceiver-Lv126	GeneCopoeia	EX-EGFP-Lv126

(*Continued on next page*)

Continued

REAGENT or RESOURCE	SOURCE	IDENTIFIER
ORF expression clone for mouse PPARA(L02932.1) (Lenti viral, CMV, Purified plasmid)	GeneCopoeia	EX-G0109-Lv126
MERCK mission shRNA bacterial stock for human PDK1	Sigma-Aldrich	TRCN0000006261, TRCN0000194672, TRCN0000196728, TRCN0000196891, TRCN0000006260
MERCK mission shRNA bacterial stock for human PDK2	Sigma-Aldrich	TRCN0000002314, TRCN0000002315, TRCN0000002316, TRCN0000002317, TRCN0000002318
Acetyl CoA synthetase (ACSS2) (NM_018677) Human Tagged ORF Clone	Origene	RC204260
pGL4.10[luc2] luciferase reporter	Promega	PAE6651
pNL1.1.TK[Nluc/TK]	Promega	PAN1501
Biological samples		
Human paraffin-embedded tissue slides	Biomax	BCN721b, BCN801, BCN963b
Human: gene expression from RNA sequencing	Cancer Genome Atlas (TCGA)	https://cancergenome.nih.gov
Chemicals, peptides, and recombinant proteins		
PBS	Sigma-Aldrich	D8537
Puromycin	Gibco	A11138-03
Trypsin-EDTA	Sigma-Aldrich	T3924
FBS	Gibco	10500064
1% penicillin/streptomycin	Thermo Fisher	15140122
DMEM	Sigma-Aldrich	D5671
L- glutamine	Gibco	25030081
1x EDTA-free protease inhibitor Cocktail	Roche	11836170001
RNase inhibitor	Promega	N261B
Fast SYBR Green master mix	Applied Biosystems	4385612
iScript cDNA synthesis kit	Bio-Rad	1708891
Bovine serum albumin	PanReac AppliChem	A6588,0100
PMSF	Merck	10837091001
SuperSignal West Femto Maximum Sensitivity Substrate	Thermo Fisher	34095
SuperSignal West Pico Chemiluminescent Substrate	Thermo Fisher	30480
T4 DNA Ligase	NEB	M0202S
RNeasy Mini Kit (50)	Qiagen	74104
RNase-Free DNase Set (50)	Qiagen	79254
Sequencing-grade modified trypsin	Worthington	N/A
Endoproteinase LysC	Waco	N/A
C18 reverse-phase SepPak-200mg columns	Waters	N/A
PhosSTOP	Roche	04906837001
Nonessential amino acids	Thermo Fisher	11140050
Sodium pyruvate	Gibco	11360070
T-PER	Thermo Fisher	78510
Sucrose	Sigma-Aldrich	S0389
Mannitol	Merck	105980

(*Continued on next page*)

Continued

REAGENT or RESOURCE	SOURCE	IDENTIFIER
Tris	Merck	GE17-1321-01
EGTA	Merck	324626
M-PER	Thermo Fisher	78501
4% w/v formalin solution	J.T. Baker	N/A
EDTA	Sigma-Aldrich	E9884
Sodium azide	Sigma-Aldrich	S2002
Matrigel	BD biosciences	N/A
NaCl	Merck	S9888
TERGITOL™ solution (NP-40)	Sigma-Aldrich	NP40S-100ML
Acetyl-lysine antibodies immobilized to agarose beads	Immunochem	ICP0388-5mg
Rabbit IgG control agarose	Novus	NBP-97118
Control agarose bead	Thermo Fisher	2150
Protein A/G magnetic beads	Pierce	88803
Purified rabbit IgG	Bethyl	P120-101
JetPRIME	polyplus	101000046
X-tremeGENE 360	Sigma-Aldrich	8724121001
DMEM/F12	Gibco	11320033
Insulin-Transferrin-Selenium (ITS -G) (100X)	Gibco	41400045
Dexamethasone	Sigma-Aldrich	D2915
Aceto acetate	Sigma-Aldrich	A8509
Keto valine	Sigma-Aldrich	198994
Keto iso-leucine	Sigma-Aldrich	K7125
DCA	Santacruz Biotechnology	sc203275
Verteporfin	Sigma-Aldrich	SML0534
perchloric acid	Merck	244252
Urea	Applichem	A1086
Trichostatin A (TSA)	Sigma-Aldrich	T1952
Dithiothreitol (DTT)	Sigma-Aldrich	D0632
2-Chloroacetamide (CAA)	Sigma-Aldrich	22790
Trifluoroacetic acid (TFA)	Applied Biosystems	N/A
Bovine Serum Albumin	Sigma-Alrdich	A9647
ImmPACT NovaRED substrate, peroxidase (HRP)	Vector Laboratories	SK-4805
Hematoxylin and Eosin	Vector Laboratories	H-3502
Crystal violet	Sigma-Aldrich	HT90132
Critical commercial assays		
Nano-Glo dual luciferase reporter assay kit	Promega	N1610
Acetyl-CoA assay kit	Sigma-Aldrich	MAK039
PDH enzyme activity microplate assay kit	Abcam	ab109902
Glycolysis assay	Abcam	ab197244
Luminescent ATP detection assay kit	Abcam	ab113849
Cellular ROS assay kit	Abcam	ab113851
VECTASTATIN Elite ABC HRP kit, Peroxidase	Vector Laboratories	PK-6104
Deposited data		
HCC patients sequencing data	Ng et al.[19]	EGAS00001005073, EGAS00001005074
HCC patients proteome data	Ng et al.[19]	PRIDE (PXD025705, PXD025836)

(*Continued on next page*)

Continued

REAGENT or RESOURCE	SOURCE	IDENTIFIER
Mouse transcriptome sequencing data	Dimitrakopoulos et al.[12]	SRP156216
Mouse proteome data	Dimitrakopoulos et al.[12]	https://github.com/cbg-ethz/netics/tree/master/mouse_data
Mouse acetylome data	This paper	PRIDE (PXD036203)
Raw data (immunoblots, microscopy images)	This paper	https://data.mendeley.com/datasets/sn5fggcp9v/draft?a = 6ed164ed-0ca8-4366-97e8-65afed2f85d5 https://doi.org/10.17632/sn5fggcp9v.1
Experimental models: Cell lines		
Stable TEAD1,3,4 knockdown Huh7 cells	Prof. Gerhard Christophori (University of Basel, Switzerland)	N/A
HEK293T	ATCC	CRL-3216
SNU449	Prof. Diego Calvisi (University of Sassari, Italy)	N/A
Huh1 and Huh7	Prof. Gerhard Christophori (University of Basel, Switzerland)	N/A
CB1	Prof. Michael N. Hall, (University of Basel, Switzerland)	N/A
Experimental models: Organisms/strains		
Mouse: *Tsc1$^{loxP/loxP}$; Pten$^{loxP/loxP}$; Alb-Cre (L-dKO)*	Guri et al.,[13] Hindupur et al.[14]	N/A
Mouse: *Tsc1$^{loxP/loxP}$; Pten$^{loxP/loxP}$ (Control)*	Guri et al.,[13] Hindupur et al.[14]	N/A
Mouse: NOD/SCID gamma-c (NSG)	The Jackson Laboratory	JAX:005557
Oligonucleotides		
ACAA2 Forward primer	TGCGTTTTGGAACCAAGC	N/A
ACAA2 Reverse primer	CATGCTGATCTGTTAATGATACCC	N/A
ACAD8 Forward primer	CTCCAAGTCCTGCCACA	N/A
ACAD8 Reverse primer	CCAGAGGCTCTCCAAACTGCTT	N/A
ACADVL Forward primer	TAGGAGAGGCAGGCAAACAGCT	N/A
ACADVL Reverse primer	CACAGTGGCAAACTGCTCCAGA	N/A
ACAT1 Forward primer	TTGATACATAACTCCGTTCCACA	N/A
ACAT1 Reverse primer	GACCATGGCTGTGCTGG	N/A
ACSL1 Forward primer	CTTCTGGTACGCCACGAGAC	N/A
ACSL1 Reverse primer	GTCGCTGTCAAGTAGTGCG	N/A
Actin Forward primer	GCGAGAAGATGACCCAGATC	N/A
Actin Reverse primer	CCAGTGGTACGGCCAGAGG	N/A
AUH Forward primer	CCAGTGAAGTTGGTCCTTTTGTC	N/A
AUH Reverse primer	GCTAAAGCCAGTTCAAGACCACC	N/A
BDH1 Forward primer	GAAAGTGGTGGAGATTGTCCGC	N/A
BDH1 Reverse primer	TGTAGGTCTCCAGGCTGGTGAA	N/A
E2A Forward primer	CCGACTCCTACAGTGGGCTA	N/A
E2A Reverse primer	CGCTGACGTGTTCTCCTCG	N/A
ECHS1 Forward primer	TTTTCTGCGATGATGTACTCAAA	N/A
ECHS1 Reverse primer	CTGCGTGTCCTGCTGTCCT	N/A
GAPDH Forward primer	AGCCACATCGCTCAGACA	N/A
GAPDH Reverse primer	GCCCAATACGACCAAATCC	N/A
HIBCH Forward primer	GGAGTTGGTCTCTCAGTCCATG	N/A
HIBCH Reverse primer	CCAAGTTTTCCTTGGAGTCGTGG	N/A
HMGCL Forward primer	TGCTGTCATGCAGGAAGTGCCT	N/A

(*Continued on next page*)

Continued

REAGENT or RESOURCE	SOURCE	IDENTIFIER
HMGCL Reverse primer	CTCCAAGTCCTGCCACA	N/A
IVD Forward primer	ACACCATTCCCTACCTGCACGT	N/A
IVD Reverse primer	ACATACTGCCGACACGCCATGA	N/A
MCCC1 Forward primer	AGCAGACCCTTCCACCAGGATT	N/A
MCCC1 Reverse primer	CACACGACCAGCTTCGCAATCA	N/A
NANOG Forward primer	CAAAGGCAAACAACCCACTT	N/A
NANOG Reverse primer	TCTGCTGGAGGCTGAGGTAT	N/A
OCT4 Forward primer	TTTTGGTACCCCAGGCTATG	N/A
OCT4 Reverse primer	GCAGGCACCTCAGTTTGAAT	N/A
PDK1 Forward primer	CATGTCACGCTGGGTAATGAGG	N/A
PDK1 Reverse primer	CTCAACACGAGGTCTTGGTGCA	N/A
PDK2 Forward primer	TGCCTACGACATGGCTAAGCTC	N/A
PDK2 Reverse primer	GACGTAGACCATGTGAATCGGC	N/A
SALL4 Forward primer	ACATCTCCGCGGTGGATGT	N/A
SALL4 Reverse primer	TGCTCCGACACTTGTGCTTG	N/A
SOX2 Forward primer	GAGCTTTGCAGGAAGTTTGC	N/A
SOX2 Reverse primer	GCAAGAAGCCTCTCCTTGAA	N/A
TEAD1 Forward primer	ATGCCAACCATTCTTACAGTGAC	N/A
TEAD1 Reverse primer	ACAGTTCCTTTAAGCCACCTTTC	N/A
TEAD2 Forward primer	GACGGCAGATTTGTGTACCG	N/A
TEAD2 Reverse primer	GAGACCTCGAAGACATAGGCG	N/A
TEAD3 Forward primer	TCATCCTGTCAGACGAGGG	N/A
TEAD3 Reverse primer	TCTTCCGAGCTAGAACCTGTATG	N/A
TEAD4 Forward primer	GAACGGGGACCCTCCAATG	N/A
TEAD4 Reverse primer	GCGAGCATACTCTGTCTCAAC	N/A
mE2a Forward primer	GGGTGCCAGCGAGATCAAG	N/A
mE2a Reverse primer	ATGAGCAGTTTGGTCTGCGG	N/A
mGapdh Forward primer	GCACAGTCAAGGCCGAGAAT	N/A
mGapdh Reverse primer	GCCTTCTCCATGGTGGTGAA	N/A
mTead2 Forward primer	GAAGACGAGAACGCGAAAGC	N/A
mTead2 Reverse primer	GATGAGCTGTGCCGAAGACA	N/A
mTead3 Forward primer	TGGACAAGGGTCTGGACAACG	N/A
mTead3 Reverse primer	AACCTTGAGGAGGAGGAGAAG	N/A
mTead4 Forward primer	ATTACCTCCAACGAGTGGAGC	N/A
mTead4 Reverse primer	CTGGCAAAGCTCCTTGCCAAA	N/A
		N/A
Recombinant DNA		
pGL4.1[luc2]-ACAD8 promoter region	This paper	N/A
pGL4.1[luc2]-ACAA2 promoter region	This paper	N/A
pGL4.1[luc2]-CPT2 promoter region	This paper	N/A
pGL4.1[luc2]-IVD promoter region	This paper	N/A
Software and algorithms		
GraphPad Prism 9	https://www.graphpad.com/scientific-software/prism/	N/A
Fiji	https://fiji.sc/#cite	N/A
ZEN 2 (blue edition)	Carl Zeiss	N/A
FlowJo	https://www.flowjo.com	N/A
Tecan i-control, version 1.11.1.0	Tecan	N/A

(*Continued on next page*)

Continued

REAGENT or RESOURCE	SOURCE	IDENTIFIER
Progenesis QI v2.0, Nonlinear dynamics Limited	http://www.nonlinear.com/progenesis/	N/A
MaxQuant v1.0.13.13	http://www.coxdocs.org/doku.php?id = maxquant:start	N/A
JASPAR	http://jaspar.genereg.net/	N/A
Other		

RESOURCE AVAILABILITY

Lead contact

Requests for information and reagents should be directed to and will be fulfilled by the lead contact, Michael N. Hall (m.hall@unibas.ch).

Materials availability

All unique/stable reagents and data generated in this study are available from the lead contact without restriction.

Data and code availability

Original western blot and microscopy images have been deposited at Mendeley Data, which are publicly available as of the date of publication. Proteomic, transcriptomic, and metabolomic data has been deposited to ERAS, PRIDE, SRP, github, and Mendeley. Links are provided in the key resources table.

This paper does not report original code.

Any additional information required to reanalyze the data reported in this paper is available from the lead contact upon request.

EXPERIMENTAL MODEL AND SUBJECT DETAILS

Animals

Liver-specific *Tsc1* and *Pten* double-knockout mice were obtained by crossing $Tsc1^{loxP/loxP}$ mice with $Pten^{loxP/loxP}$ mice expressing Cre recombinase under the control of hepatocyte-specific albumin promoter. Age-matched littermate $Tsc1^{loxP/loxP}$ $Pten^{loxP/loxP}$ mice without the *Cre* gene were used as controls. Mice had a mixed genetic background (C57BL/6J, 129/SvJae, BALB/cJ). Mice were housed in temperature and humidity-controlled conditions, in a 12h light/dark cycle. All experiments were conducted on male mice. Prior to all experiments, mice were fasted overnight. All relevant ethical regulations were followed. The tumors were harvested at 20 weeks of age. Also, the condition of mice was monitored according to a score sheet as stipulated by the Institutional Animal Care and Use Committee (IACUC), Kantonales Veterinäramt of Kanton Basel-Stadt. For all animal experiments, respecting animal ethics rules, a minimal number of animals was used as required to get a statistically meaningful result. All animal experiments were performed under the federal ethical guidelines and were approved by the Kantonales Veterinäramt of Kanton Basel-Stadt.

Human and mouse HCC cell lines

SNU449 cell line was kindly provided by Prof. Diego Calvisi (University of Sassari, Italy). Huh1 and Huh7 cell lines were kindly provided by Prof. Gerhard Christophori (University of Basel, Switzerland). CB1 cells were established from 20 week old L-dKO tumors in our laboratory.[14] All cell lines used in the study were tested and found free of mycoplasma contamination. All cell lines were grown in DMEM high glucose media supplemented with 10 % FBS, glutamine, nonessential amino acids, sodium pyruvate, and penicillin-streptomycin. Ultra-low attachment six-well plates (Corning, 3471) were used for hepatosphere formation assay.

Patient material and ethics

All relevant ethical regulations were followed in this study. Human tissues were obtained from patients undergoing diagnostic liver biopsy at the University Hospital Basel, between 2008 and 2018. Written informed consent was obtained from all patients. The study was approved by the ethics committee of the northwestern part of Switzerland (Protocol Number EKNZ 2014-099). Ultrasound-guided needle biopsies were obtained from tumor lesion(s) and the liver parenchyma at a site distant from the tumor, following a co-axial liver biopsy technique that allows obtaining several biopsy samples through a single biopsy needle tract as described.[76] Clinical disease staging was performed using the Barcelona Clinic Liver Cancer system.[77] Biopsies from multicentric tumors (i.e., genetically independent primary tumors) but not intra-hepatic metastases were included. In total, 122 HCC biopsies and 115 non-tumoral tissues from 114 patients were included in the study, including 6 patients from whom 2 synchronous multicentric tumor biopsies and 1 patient from whom 3 multicentric tumor biopsies were obtained. Regarding etiology, main etiologies were chronic alcoholism

(alcoholic liver disease, ALD) (68 patients), HBV or HCV infection (43 patients), and non-alcoholic fatty liver disease (NAFLD) (19 patients). None of the patients had received systemic or locoregional therapies for liver cancer prior to biopsy. Two patients were treated with curative surgery or ablation and were biopsied after HCC recurrence was diagnosed by imaging. The ethics committee approved all experiments with resected human tissue samples (EKNZ, approval No. 361/12).

METHOD DETAILS

Immunoblot analysis

Liver tissues were homogenized in T-PER supplemented with 1 mM PMSF, 1× Complete Mini Protease Inhibitors, 1× PhosSTOP using a Polytron (PT 10-35 GT). For subcellular fractionation, homogenized liver lysates were solubilized with buffer A (225mL mannitol, 75mM sucrose, 30mM tris-Cl pH 7.4, 0.5mM EGTA) and incubated on ice 10min. The nuclear pellet was obtained after centrifugation (200g, 5min, at 4°C) and solubilized in M-PER buffer after three times washing with PBS. The mitochondrial pellet was obtained after centrifugation (12000g, 15min, at 4°C) and solubilized in M-PER buffer after three times washing with PBS. The cytoplasmic fraction was recovered after centrifugation (15000g, 10min, at 4°C).

For the lysis of cells, an M-PER buffer was used. Equal amounts of homogenates were separated by SDS–PAGE and transferred onto a nitrocellulose membrane (GE Healthcare)

H&E staining and immunohistochemistry (IHC)

The livers were fixed in 4% w/v formalin solution, dehydrated, and embedded into paraffin wax blocks. Embedded tissues were cut into 4μm thick sections placed on superFrost slides (Thermo Scientific) and stained with hematoxylin and eosin (H&E). IHC was performed using the acetyl-lysine antibodies. For tumor microarray (TMA) analysis, we used human paraffin-embedded tissue slides and performed IHC using anti-acetyl-lysine antibodies.

Fluorescence activated cell sorting (FACS)

Confluent CB1 cells were dissociated with trypsin and washed twice in FACS buffer (PBS, 2% FBS, 5mM EDTA, 0.1% sodium azide). Cells were labeled with Alexa 555 conjugated anti-CD44 antibody at 4°C for 20min. Cells were washed twice in FACS buffer and filtered with a 0.2μm syringe filter. Brightly and weakly stained cells were separated as gated by FACS (BD FACSAria™ Fusion Flow Cytometers) and were designated as CD44 high or CD44 low cells, respectively.

HCC xenografts in NOD/SCID gamma-c (NSG) mice

Xenograft experiments were performed with male NSG mice (8-week-old). $3x10^6$ Huh7 cells were resuspended in Matrigel and injected into a mouse's right (double-knockdown cells) and left (control cells) flank. Tumor size was measured every 2-5 days using a caliper slide rule. Tumor volume was calculated as follows: Tumor volume = 3.14159 x (longest diameter x shortest diameter2)/6. Tumors were harvested when they reached more than 450 mm^3 in volume (33 days or 40 days after injection). Tissue samples were snap frozen or fixed in formalin. The animal experiments were performed strictly according to Swiss federal ethical guidelines and were approved by the Kantonales Veterinäramt of Kanton Basel-Stadt.

Immunoprecipitation (IP)

Frozen L-dKO tumors and livers from littermate controls were pulverized in a metal mortar cooled on dry ice. Powdered tissues were resuspended in 50mM Tris-HCl (pH 8.0), 100mM NaCl, 1mM PMSF, 1mM EDTA, 0.5% NP-40, 1x complete mini protease inhibitor, 1x PhosSTOP (hereafter referred to as IP buffer) and homogenized using a Polytron at 15000rpm for 30sec. Lysates are incubated at 4°C on a rotator for 20min and centrifugated at 15000g for 10min at 4°C to remove cell debris. Protein concentration in the supernatant was determined using the BCA assay. Tissue lysates from three different animals were pooled. For immunoprecipitation from SNU449 cells, the same IP buffer and process were used. For immunoprecipitation of acetylated proteins, anti-acetyl lysine antibodies immobilized on agarose beads were used. 100ul of beads were incubated with 1mg of lysate in 1ml of IP buffer for four hours at 4°C with gentle rotation. After washing 4 times, the bound acetylated proteins were eluted with 2x Laemmli buffer and resolved by SDS-PAGE for subsequent immunoblot analysis. Rabbit IgG control agarose was used as the negative control. Before IP, the lysates were pre-cleared with a control agarose bead. For immunoprecipitation of OCT4 or SOX2 proteins, 1mg of lysate was incubated with 20μl of antibody for two hours at 4°C with gentle rotation. Next, 20μl of Pierce protein A/G magnetic beads were added and incubated overnight at 4°C with gentle rotation. After four washes, bound protein was eluted with 2x Laemmli buffer and resolved by SDS-PAGE for subsequent immunoblot analysis. Purified rabbit IgG was used as the negative control. Lysates were pre-cleared with protein A/G magnetic beads for one hour at 4°C with gentle rotation.

Stable TEAD2 or E2A overexpression or knockdown cells

For lentivirus generation, $2x10^6$ HEK293T cells were seeded in a 10cm dish in DMEM supplemented with 10% FBS the day before transfection. Cells were transfected by JetPRIME. Medium was exchanged with fresh medium six hours after transfection. After 24hours and 48hours, the supernatant was recovered and filtered with 0.2 μm filters and used to infect HCC cell lines. Stable transfected cell lines were obtained by puromycin or blasticidin selection. After antibiotic selection, single-cell clones were generated for further use.

Stable *PDK1* and *PDK2* knockdown cells

Lentiviral particles were generated as described above. Stable cell lines were obtained by puromycin selection.

Transient ACSS2 overexpression cells

Cells were transfected by JetPRIME and harvested after 48 hours. For clonogenic growth assay, Cells were transfected every third day and harvested after one week.

Transient transfection and luciferase reporter constructs

Transient gene transfection was carried out to assess the effect of TEAD2 and/or E2A on luciferase reporters in SNU449 cells. 10^4 cells were seeded in 96 well plate and transfected with the firefly pGL4.10[luc2] luciferase reporter vector containing a ~1000bp promoter region of an acetyl-CoA synthesis gene (*ACAD8*, *ACAA2*, *CPT2*, or *IVD*) together with pNL1.1.TK[Nluc/TK] internal control vector, by X-tremeGENE 360. Nano-Glo dual luciferase reporter assay kit was used to measure the reporter activity according to the manufacturer's instructions 48 hours post-transfection. Luciferase activity was normalized by using a pNL1.1.TK[Nluc/TK] internal control.

Cell treatments

For acetyl-CoA replenishing reagent (ARR) treatment, cells were cultured in DMEM supplemented with 2mM aceto acetate, 2mM keto valine, 2mM keto isoleucine, and 4mM DCA. For verteporfin treatment, cells were cultured in DMEM supplemented with 5 or 10uM verteporfin for 24 hours.

Clonogenic growth assay and crystal violet staining

CB1 (10^3 cells per well) and other HCC cell lines (10^4 cells per well) were seeded in a six-well plate and stained with crystal violet (2% crystal violet in 20% methanol) after seven days ($n \geq 3$). Absorbance was measured at 560 nm on a Tecan Infinite M1000 machine. The software Tecan i-control, version 1.11.1.0, was used according to the manufacturer's instructions. Blank was set with a stained 6-well plate without cells. Multiple reads were read per well (15 × 15 reads), and a border of 3,000 μm was left in each well. The number of flashes was set to 25 with 10ms of settle time.

RNA isolation and quantitative reverse transcriptase PCR

Total RNA was isolated with TRIzol Reagent and RNeasy Kit. RNA was reverse transcribed to cDNA using an iScript cDNA Synthesis Kit. Quantitative real-time PCR analysis was performed using Fast SYBR Green and q^3TOWER (Analytik Jena). Relative expression levels were determined by normalizing each Ct value to *Gapdh* expression for mice and *Actin* or *GAPDH* for human samples and HCC cell lines using the ΔΔCt method. For each gene at least three independent biological replicates were used. Primer pairs used in this study are listed in STAR Methods, key resources table.

Metabolites and enzyme activity assays

Acetyl-CoA was measured using an assay kit. Cells or tissues were harvested in assay buffer provided by the assay kit and homogenized. The protein was precipitated with perchloric acid (PCA). After centrifugation, the supernatant was recovered and neutralized by adding potassium bicarbonate until the pH of the sample was in the range of 6-8, and the precipitant was removed by centrifugation. The supernatant was used to determine acetyl-CoA concentration in more than triplicate with the acetyl-CoA assay kit according to the manufacturer's instructions. Pyruvate dehydrogenase complex (PDC) enzyme activity was measured using a PDH enzyme activity microplate assay kit. Tissues were harvested in the provided detergent solution and protein concentration was measured using the BCA assay. The same amount of protein was used for each PDH activity measurement according to the manufacturer's instructions.

For ECAR, ATP, and ROS measurements, cells were seeded in 96 a well plate at recommended density, and measurements were performed using a glycolysis assay, luminescent ATP detection assay kit, and cellular ROS assay kit, respectively, according to the manufacturer's instructions. For extracellular lactate measurement, $5x10^5$ cells were seeded in a 12 well plate, and 2ul of conditioned medium was used for measurement using lactate pro 2 (Axonlab) after 24 hours.

Mouse proteome and transcriptome

12 frozen tumors from four L-dKO mice and six frozen control livers from littermates were used for proteomic and transcriptomic analysis.[12,14] For subsequent analysis, we computed the $\log_2$-fold-change in protein abundance in tumors compared to control livers.

Mouse acetylome

Frozen L-dKO tumors and control livers from littermate control mice (CTRL) were pulverized in a metal mortar cooled on dry ice. Powdered tissues were resuspended in 8M urea (containing 50mM Tris-HCl (pH 8.0), 150mM NaCl, 1mM PMSF, 1x Complete Mini Protease Inhibitors, 1x PhosSTOP, 2μM TSA) and homogenized using a Polytron at 15000rpm for 30sec. Lysates are incubated at 4°C on a rotator for 20min and centrifugated at 15000g for 10min at 4°C to remove cell debris. Protein concentration in

the supernatant was determined using Bradford assay. Tissue lysates from three or four different animals was pooled and reduced with 10mM dithiothreitol (DTT) for one hour at 37°C, cooled for 5–10min at room temperature, and alkylated with 50mM 2-Chloroacetamide (CAA) for 30min at room temperature in dark. The urea concentration was reduced to 3M by diluting with 50mM Tris-HCl, pH 8.0. Proteins were treated with endoproteinase LysC (1:100; w/w) at 37 °C for four hours. The urea concentration of the LysC digest was reduced to 1M. Later, trypsin digestion (1:50; w/w) was performed overnight at 37 °C. Digestion was stopped by adding 0.5% trifluoroacetic acid (TFA) (v/v) that lowered the pH of the solution to below pH 2.0. Later, the digest was centrifuged at 10,000g for 10min at room temperature and the supernatant was desalted on a C18 reverse-phase SepPak-200mg column. The peptides were dried in a SpeedVac and resuspended in IP buffer. Acetylated lysine peptides were enriched using acetyl lysine antibody immobilized to agarose beads in a 1:20 antibody:peptides ratio. The samples were incubated overnight at 4°C with gentle rotation and then rinsed three times with IP buffer and three times with water, followed by elution with 0.1% TFA. Eluted peptides were desalted before analysis. Aliquots containing either 1ug of peptides were subjected to label-free quantification-based LC-MS analysis. The setup of the μRPLC-MS system was as described previously.[78] Chromatographic separation of peptides was carried out using an EASY nano-LC 1200 system (Thermo Fisher Scientific), equipped with a heated RP-HPLC column (75 μm x 37 cm) packed in-house with 1.9μm C18 resin (Reprosil-AQ Pur, Dr. Maisch). Peptides were analyzed per LC-MS/MS run using a linear gradient ranging from 95% solvent A (0.15% formic acid, 2% acetonitrile) and 5% solvent B (98% acetonitrile, 2% water, 0.15% formic acid) to 30% solvent B over 90minutes at a flow rate of 200nl/min. Mass spectrometry analysis was performed on an Orbitrap Fusion Lumos Tribrid LC-MS platform equipped with a nanoelectrospray ion source (Thermo Fisher Scientific). Each MS1 scan was followed by high-collision-dissociation (HCD) of the most abundant precursor ions using a cycle time of 3seconds with a dynamic exclusion for 20seconds. For MS1, 4E5 ions were accumulated in the Orbitrap cell over a maximum time of 100ms and scanned at a resolution of 240,000 FWHM (at 200m/z). MS2 scans were acquired in the build in ion trap using a normalized collision energy of 30%, a target setting of 10E4 ions and an accumulation time of 25ms. Singly charged ions and ions with unassigned charge state were excluded from triggering MS2 events. The mass isolation window was set to 1.4m/z and one microscan was acquired for each spectrum. The acquired raw-files were imported into the Progenesis QI software (v2.0, Nonlinear Dynamics Limited), which was used to extract peptide precursor ion intensities across all samples applying the default parameters. The generated mgf-files were searched using MASCOT against a decoy database containing normal and reverse sequences of the predicted SwissProt entries of *mus musculus* (www.ebi.ac.uk, release date 2016/11/15) and commonly observed contaminants (in total 33,984 sequence entries) generated using the SequenceReverser tool from the MaxQuant software (Version 1.0.13.13). The search criteria were set as follows: full tryptic specificity was required (cleavage after lysine or arginine residues, unless followed by proline); three missed cleavages were allowed; carbamidomethylation (C) was set as fixed modification; oxidation (M) and acetylation (K) were applied as variable modifications; mass tolerance of 10 ppm (precursor) and 0.6 Da (fragments). The database search results were filtered using the ion score to set the false discovery rate (FDR) to 1% on the peptide and protein level, respectively, based on the number of reverse protein sequence hits in the datasets. The relative quantitative data obtained were normalized and statistically analyzed using our in-house script as above.[78] The mass spectrometry proteomics data have been deposited to the ProteomeXchange Consortium via the PRIDE partner repository with the dataset identifier PXD036203 and 10.6019/PXD036203.

Metabolomics of mouse liver tissues

Snap-frozen liver samples from CTRL and L-dKO mice were collected and weighed. (WT: n=5, weight mean = 53.7mg, stdev =4.2 mg; L-dKO: n=6, weight mean = 55mg, stdev = 11.4.) Sample weights did not differ significantly between the two groups (two-tailed t-test, unequal variances p-value = 0.81). Metabolite extraction was performed previously described.[45] Tissue samples were kept on dry ice and homogenized in 1ml of 70% ethanol using a Tissue Lyser 2 (Qiagen) with a stainless steel bead at maximum speed for one minute. Metabolites were extracted from the homogenized samples by adding 7ml of 70% ethanol heated to 75°C for 2minutes and subsequently cooled in ice water. Extracts were separated from cell debris by centrifuging at 2500g at 4°C for 10minutes, dried in a SpeedDry Vacuum Concentrator (Christ), and resuspended in double-distilled water (ddH_2O) corresponding to the measured weight, and then diluted 1:10 in ddH_2O prior to mass spectrometric analysis. Untargeted metabolomics was performed by flow injection analysis on an Agilent 6550 quadrupole instrument time-of-flight mass mass spectrometer as described previously.[79] The instrument was operated in positive mode, high-resolution (4GHz) mode. The injection sequence of samples was randomized, and all samples were injected in duplicates. Mass spectrometry data were pre-processed to collapse the time dimension, centroided, and merged into a single data matrix. Based on their accurate mass and the Human Metabolome Database reference list, Ions were annotated, allowing tolerance of 0.003 amu and multiple common ESI adducts. Annotated ions were then filtered for H+ adducts.

Proteome of patient tumor tissue

Fresh liver biopsies from 49 HCC were immediately snap-frozen in liquid nitrogen and processed as previously described[13,80] and used for proteomic analysis.[19] Human HCC biopsies were measured by sequential window acquisition of all theoretical mass spectra (SWATH), in which data-independent acquisition is coupled with spectral library match.[81] log_2-fold-changes of protein abundance in tumors compared to non-tumor tissues from the same patient were computed for further analysis.

RNA-sequencing and data processing of patient samples

RNA-seq library prep was performed with 200ng total RNA using the TruSeq Stranded Total RNA Library Prep Kit with Ribo-Zero Gold (Illumina) according to the manufacturer's specifications. $\log_2$-fold-changes of normalized RSEM gene counts of tumors compared to matched non-tumor livers were computed for further analysis. RNA-sequencing data[19] of the human HCCs are available at the European Genome-phenome Archive under accession EGAS00001005074.

Patient survival analyses

For patient survival analysis, RNA seq data from 325 HCC, 350 RCC, 488 HNSCC, 461 LSCC, 520 CRC, and 348 RNCC were retrieved from The Cancer Genome Atlas dataset (TCGA, Provisional) using the cbioportal (http://www.cbioportal.org, accessed 1 April 2021) website. Up-regulation of *TEAD2/E2A* and upregulation of dedifferentiation (stemness) markers (average expression of *CD44, SALL4, OCT4, NANOG, SOX2*, and *SOX4*) were defined as z-score $\geq$ 0.5. Down-regulation of acetyl-CoA synthesis enzymes (average expression of *IVD, MCCC1, MCCC2, AUH, HMGCL, ACADSB, ECHS1, HIBCH, HIBADH, HCD2, ACAA2, ACSL1, ACADVL, HADH, ACAT1, BDH1, ALDH2*, and *ACSS2*) was defined as z-score ≤ -0.5.

Correlation with *TEAD2* or *E2A* and binding site prediction

Pearson's correlation coefficient was used to test for associations of acetyl-CoA synthesis enzymes with *TEAD2* or *E2A* using the transcriptomes of HCC patients. Potential binding sites for TEAD2 or E2A in the promoters of acetyl-CoA synthesis genes were identified with the JASPAR database (http://jaspar.genereg.net/).

QUANTIFICATION AND STATISTICAL ANALYSIS

To determine the statistical significance between the two groups, an unpaired two-tailed Student's t-test or multiple t-tests was performed. Statistical analyses and data plotting were performed using GraphPad Prism 9 (GraphPad Software). Unless mentioned otherwise, statistical significance was defined as <0.05. An unpaired t-test assuming Gaussian distribution was used to compare between two groups. Data represent mean ± SEM. Sample numbers are indicated in each figure legend.